Hyperbaric oxygen therapy ameliorates pathophysiology of 3xTg-AD mouse model by attenuating neuroinflammation

Ronit Shapira [a], Beka Solomon [b,c], Shai Efrati [d,e], Dan Frenkel [a,c], Uri Ashery [a,c,*]

[a] Department of Neurobiology, The George S. Wise Faculty of Life Sciences, Tel Aviv University, Tel Aviv, Israel
[b] Department of Molecular Microbiology and Biotechnology, The George S. Wise Faculty of Life Sciences, Tel Aviv University, Tel Aviv, Israel
[c] Sagol School of Neuroscience, Tel Aviv University, Tel Aviv, Israel
[d] Sackler School of Medicine, Tel Aviv University, Tel Aviv, Israel
[e] Sagol Center for Hyperbaric Medicine & Research, Assaf Harofeh Medical Center, Tel Aviv, Israel

ARTICLE INFO

ABSTRACT

There is a real need for new interventions for Alzheimer's disease (AD). Hyperbaric oxygen therapy (HBOT), the medical administration of 100% oxygen at conditions greater than 1 atmosphere absolute, has been used successfully to treat several neurological conditions, but its effects on AD pathology have never been thoroughly examined. Therefore, we exposed old triple-transgenic (3xTg) and non-transgenic mice to HBOT followed by behavioral, histological, and biochemical analyses. HBOT attenuated neuroinflammatory processes by reducing astrogliosis, microgliosis, and the secretion of proinflammatory cytokines (IL-1β and TNFα) and increasing expression of scavenger receptor A, arginase1, and antiinflammatory cytokines (IL-4 and IL-10). Moreover, HBOT reduced hypoxia, amyloid burden, and tau phosphorylation in 3xTg mice and ameliorated their behavioral deficits. Therefore, we suggest that HBOT has multifaceted effects that reduce AD pathologies, even in old mice. Given that HBOT is used in the clinic to treat various indications, including neurological conditions, these results suggest HBOT as a novel therapeutic intervention for AD.

© 2017 Elsevier Inc. All rights reserved.

1. Introduction

Dementia is a common and growing problem, affecting 47.5 million people worldwide. Alzheimer's disease (AD), the most common form of dementia in the elderly, accounts for 60%—70% of cases. Globally, the number of people living with dementia is expected to escalate to 65.7 million by 2030 and 115.4 million by 2050, based on current rates of mortality and treatment availability (Prince et al., 2013). Despite many advances in our understanding of the pathophysiology of AD in the last decades, management is still mainly symptomatic, and there is a real need for new interventions.

The main pathological hallmarks characterizing AD are extracellular amyloid plaques, intracellular accumulation of neurofibrillary tangles, and progressive loss of synapses and neurons (Braak and Braak, 1997; Heinonen et al., 1995; Jellinger and Bancher, 1996). Another major component of AD is neuroinflammation. Microglia and astrocytes are key players in the inflammatory response and have been shown to be altered in postmortem brains of patients with AD and in animal models of the disorder (Hoozemans et al., 2006; Nazem et al., 2015). In early stages of the disease, the acute inflammatory response is thought to mitigate the clearance of amyloid plaques and restore tissue homeostasis. However, in advanced stages of AD, sustained activation of microglia and astrocytes (Rama Rao and Kielian, 2015; Villegas-Llerena et al., 2015) ultimately leads to chronic neuroinflammation. Excessive activation of glia due to persistent exposure to proinflammatory cytokines induces synapse loss and neuronal degeneration (Hickman et al., 2008; Iram et al., 2016; Kitazawa et al., 2011; Shi et al., 2011).

Hypoxia is intimately entwined in the pathogenesis of AD (Zhang and Le, 2010). Following hypoxic conditions, such as cerebral ischemia and stroke, the incidence of AD and vascular dementia is greatly increased (Altieri et al., 2004; Honig et al., 2005; Schneider et al., 2003). Reduced cerebral perfusion has been observed in preclinical and early stages of AD and correlates with both structural and functional deterioration as the disease progresses (Alsop et al., 2010; Binnewijzend et al., 2013; Chao et al., 2010; Chen et al., 2011; Roher et al., 2012; Thomas et al., 2015; Tosun et al., 2010). Cerebral hypoxia may arise due to hypoperfusion and has been shown to contribute to the accumulation of β-amyloid (Aβ), hyperphosphorylation of tau, dysfunction of the blood-brain barrier, and

* Corresponding author at: Department of Neurobiology, The George S. Wise Faculty of Life Sciences, Sagol School of Neuroscience, Tel Aviv University, Tel Aviv, Israel. Tel.: +97236409827; fax: +97236407643.
E-mail address: uriashery@gmail.com (U. Ashery).

degeneration of neurons (Zhang and Le, 2010). Interestingly, hypoxia has been shown to activate microglia and astroglia and induce proinflammatory cytokine secretion, thus leading to neuronal death (Kaur et al., 2013; Lai and Todd, 2006; Teo et al., 2015; Tikka et al., 2001; Yrjanheikki et al., 1998, 1999). Therefore, reducing hypoxia and neuroinflammation might be the key to ameliorate AD pathophysiology.

Hyperbaric oxygen therapy (HBOT)—the administration of 100% oxygen at environmental pressure greater than 1 ATA—is utilized for a wide range of medical conditions in which oxygen is the rate-limiting factor for tissue recovery. This includes carbon monoxide poisoning, crush injuries, and decompression sickness (Gill and Bell, 2004; Thom, 2011). Recently, HBOT has emerged as a valuable treatment in neurological conditions (Boussi-Gross et al., 2015; Figueroa and Wright, 2015; Hadanny et al., 2015; Huang and Obenaus, 2011; Tal et al., 2015). The principal effect of HBOT is an increase in the solubility of plasma oxygen to a level sufficient to support tissues with minimal oxygen supply carried out by hemoglobin (Gill and Bell, 2004; Thom, 2011). Breathing oxygen under hyperbaric conditions has been shown to be a potent means of increasing arterial oxygen tension, as well as brain oxygen tension, thereby allowing a 6-fold increase in the amount of oxygen reaching the brain tissue (Calvert et al., 2007; Meirovithz et al., 2007; Tibbles and Edelsberg, 1996; van Hulst et al., 2003). Studies suggest that HBOT reduces intracranial pressure, improves survival, and promotes neurobehavioral recovery in traumatic brain injury patients, even years after the injury (Efrati et al., 2013; Huang and Obenaus, 2011; Lin et al., 2008; Rockswold et al., 2013; Sahni et al., 2012; Tal et al., 2015). In stroke patients, HBOT significantly improved neurological functions and life quality, even at chronic late stages after the occurrence of the stroke (Boussi-Gross et al., 2015; Efrati et al., 2013; Hadanny et al., 2015; Heneka et al., 2013). In traumatic brain injury and stroke animal models, HBOT exerted part of its beneficial effect by attenuating astrogliosis and microgliosis, suppressing proinflammatory cytokine secretion and increasing antiinflammatory cytokine secretion (Chen et al., 2014; Gunther et al., 2005; Harch, 2015; Lavrnja et al., 2015; Lim et al., 2013; Liu et al., 2013). As neuroinflammation is one of the hallmarks of AD, we examined whether HBOT can reduce it in a mouse model of AD.

Although HBOT has been shown to mitigate reduced blood flow, hypoxia, and neuroinflammation in a variety of brain disorders, its effects on AD pathology have never been thoroughly studied. We investigated the effects of HBOT on AD by exposing triple transgenic–AD (3xTg-AD) mice—a mouse model of AD—to HBOT and testing for behavioral, pathological, and biochemical changes due to the treatment. Our data suggest that HBOT ameliorates cognitive deficits; reduces the presence of hypoxia, amyloid load, and phosphorylated tau; and suppresses neuroinflammation.

2. Materials and methods

2.1. Mice

Triple-transgenic (3xTg) mice, harboring the $PS1_{M146V}$, $A\beta PP_{swe}$, and tau_{P301L} transgenes (kindly received from Prof. Frank M. LaFerla), and non-transgenic (non-Tg) C57BL/6 mice were used for this study. All animal experiments were performed in accordance with animal protocols approved by the Tel Aviv University Animal Care Committee. Every effort was made to relieve animal stress and minimize animal use. Tel Aviv University follows the international ARRIVE guiding principle for biomedical research involving animals, developed by the International Organizations of Medical

Sciences. All animals received humane care as outlined in the "Guide for the Care and Use of Laboratory Animals" prepared by the National Institute of Health.

2.2. Hyperbaric oxygen therapy

Male homozygous 3xTg mice (17-month old) and non-Tg C57BL/6 mice (14-month old) were assigned to 2 groups: HBO-treated and control non-treated mice. For the HBOT, animals were administered 100% oxygen at a pressure of 2 ATA in a custom-made monochamber intended for small animals for 60 minutes daily for 14 consecutive days (n = 14). Before compression was initiated, the monochamber was washed with 100% oxygen for 5 minutes to enrich oxygen content. Compression and decompression were performed gradually within 5 minutes. Oxygen level inside the chamber following compression reached saturation of $\geq 96\%$, as measured by an oxygen analyzer (320BRC model; Teledyne Analytical Instruments). The animals in the control, non-treated group, were placed inside the monochamber for 60 minutes without additional treatment (at 1 ATA; n = 14). Temperature, measured with a temperature controller (N322; Novus) during all sessions for HBO and control groups in the monochamber, was similar between groups (HBO: $21.64 + 0.1699\ °C$, $n = 14$, control: $21.79 + 0.1710\ °C$, $n = 14$, $p = 0.5201$).

2.3. Behavioral testing

The effects of HBOT on memory and behavior in mice were evaluated using a series of behavioral tests. Tests were performed during the 7 days preceding sacrifice with a 24-hour delay after the last HBOT/control treatment and a 48-hour delay after the last task to reduce stress.

2.3.1. Y-maze test
The test was performed in a symmetrical black Plexiglas Y maze with 3 arms (30 cm long × 10 cm wide × 15 cm high) set at 120° angles, designated entrance, familiar, and novel. The mice were placed in the distal end of the entrance arm and allowed to explore the maze for 10 minutes with only the familiar arm available to explore. After a 2-minutes delay, mice were reintroduced into the maze with 2 arms (familiar and novel) available to explore and documented for 2 minutes. The ratio of time spent or frequency of visits to the novel arm was calculated as time or frequency in the novel arm divided by the sum of time or frequency in both novel and familiar arms. The maze was cleaned with 40% ethanol between sessions. Arms were changed randomly between animals but kept similar for each animal.

2.3.2. Open-field test
Animals were placed in the center of an open field (40 cm × 40 cm × 30 cm), and exploration was assessed for 15 minutes. Cages were cleaned with ethanol following each session.

2.3.3. Novel object–recognition test
Mice were allowed to explore an empty arena (40 cm × 40 cm × 30 cm walls), and 24 hours later, 2 identical objects were added for a familiarization session of 10 minutes. Either 5 minutes (short-term memory test) or 24 hours (long-term memory test) later, the mice were reintroduced into the arena with one of the objects having been replaced by a novel one. The behavior of the mice was then monitored using the EthoVision XT 9 program for 5 minutes, and the time and number of visits to each of the objects were measured. The results are presented as the ratio of percentage of time spent

near the novel object to total time spent near both novel and the familiar objects.

2.4. Biochemical and histological analyses

Mice were anesthetized with ketamine and xylazine and perfused transcardially with phosphate-buffered saline. Their brains were then excised and halved, and each hemisphere was further processed for either biochemical or histological analysis, as outlined in the following paragraphs.

2.4.1. Immunohistochemistry and confocal microscopy

One brain hemisphere was fixed overnight with 4% para-formaldehyde in 0.1 M phosphate buffer (pH 7.4) and then placed in 30% sucrose for 48 hours. Frozen coronal sections (30 μm) were then cut on a sliding microtome, collected serially and stored in cryoprotectant (containing glycerin, ethylene glycol, and 0.1 M sodium phosphate buffer, pH 7.4) at −20 °C until use. The free-floating sections were immunostained with the following primary antibodies: biotinylated mouse anti-Aβ 17-24 (4G8, 1:200; Signet Laboratories), mouse biotinylated anti-202/205 phosphorylated tau (AT8, 1:200; Innogenetics), rabbit anti-ionized calcium-binding adapter molecule 1 (Iba1, 1:700; Waco), rabbit anti-glial fibrillary protein (GFAP, 1:400; Sigma), rat anti-tumor necrosis factor alpha (TNFα, 1:500; Abcam), and rat-anti CD204 (scavenger receptor A [SR-A], 1:400; Bio-Rad). First, sections were blocked with 10%−20% normal goat serum in PBST for 2 hours at room temperature and then incubated for 24 hours at 4 °C with the primary antibodies (dissolved in 2% w/v normal goat serum in PBST). Next, primary antibodies were visualized by incubating the sections for 1.5 hours at room temperature with Alexa Fluor 488−conjugated goat anti-rabbit (1:1000; Jackson ImmunoResearch Laboratories), Alexa Fluor 568−conjugated avidin (1:1000; Jackson ImmunoResearch Laboratories), Alexa Fluor 488−conjugated goat anti-rat (1:1000; Abcam), or Alexa Fluor 647−conjugated goat anti-rabbit (1:500; Invitrogen), depending on the primary antibody. The sections were then mounted on slides coated with dry gelatin and visualized using a confocal scanning laser microscope (LSM Meta; Zeiss). Images (1024 × 1024 pixels, 12 bit) were acquired by averaging 8 scans. Aβ staining was performed similarly, except that before blocking, the sections were incubated with 70% formic acid (FA) for 6 minutes to increase antigen retrieval before antibody staining. Images of stained brains were obtained at 10× and 40× magnifications. For subiculum analysis, 2 sections per animal at bregma −2.55 to −3.45 were analyzed (at 40× magnification, 2−4 fields of view per slice); and for hippocampal analysis, 3−4 sections per animal at bregma −1.45 to −3.28 were analyzed (at 40× magnification, 3 fields of view per slice). Control experiments revealed no staining in sections that lacked the first antibody and were used to determine the threshold for intensity quantification. Intensity of the immunofluorescent staining above threshold level was calculated with the Image-Pro Plus system (version 5.1; Media Cybernetics).

2.4.2. Protein and mRNA isolation

One brain hemisphere was snap frozen in liquid nitrogen and stored at −80 °C until use. The hippocampus was excised on ice at 4 °C, and total mRNA and protein were extracted from the tissue using the NucleoSpin RNA/protein kit (#740933; MACHEREY-NAGEL) according to the manufacturer's instructions.

2.4.3. Quantitative real-time PCR

RNA was transcribed into cDNA using the High-Capacity cDNA Reverse Transcription Kit (Applied Biosystems), and TaqMan real-time quantitative PCR assays were used according to the

manufacturer's specifications (Applied Biosystems) to quantify the mRNA expression SR-A (*msr1*, Mm00446214_m1), arginase1 (*arg1*, Mm00475988_m1), interleukin 1 beta (*IL-1β*, Mm00434228_m1), interleukin 4 (*IL-4*, Mm00445259_m1), and interleukin 10 (*IL-10*, Mm01288386_m1). Quantification was conducted using the $\Delta\Delta C_T$ method by comparing the target genes to the expression of the housekeeping gene *gapdh* (glyceraldehyde 3-phosphate dehydrogenase, Mm99999915_g1) and normalizing all samples to the non-Tg controls.

2.4.4. Immunoblotting

Proteins were dissolved in 200 μL lysis buffer containing 7.5 mM HEPES pH 7, 1.5 mM EDTA, 1.5 mM EGTA, 0.375 mM DTT, protease inhibitor cocktail (P8340; Sigma), phosphatase inhibitor cocktail (P5726; Sigma), and 25% of 10% SDS (Amresco Pure, Technology Grade), and concentrations were determined using the BCA protein assay kit (Pierce). Equal amounts of protein were separated on a 4%−20% Bis-Tris gel (Bio-Rad) and transferred to nitrocellulose membranes. Membranes were blocked overnight in 5% (w/v) nonfat milk in 0.1% Tween 20 Tris-buffered saline (TBS). After blocking, the membranes were incubated for 1 hour at room temperature with primary antibodies specified in Supplementary Material Table 1.

The membranes were then washed in Tween-TBS for 20 minutes and incubated at room temperature with specific horseradish peroxidase−conjugated secondary antibodies at a dilution of 1:15,000 (Jackson ImmunoResearch Laboratories) for 60 minutes. The immunoblot bands were developed using enhanced chemiluminescent substrate (Pierce), and their intensity was quantified with ImageQuant TL (Amersham). GAPDH levels were used to verify uniform loading of the samples across the gel.

2.4.5. Hypoxyprobe staining

Eight days after the last session of HBO or normobaric treatment, half of the mice from each treatment group were injected intraperitoneally with 60 mg/kg of Hypoxyprobe 1 (pimonidazole hydrochloride, Hypoxyprobe1, USA) 30 minutes before tissue harvesting to detect hypoxia. Pimonidazole is distributed to all tissues, including the brain, but it only forms stable adducts with thiol groups in proteins, peptides, and amino acids found in hypoxic cells under conditions of partial pressure of oxygen smaller than 10 mm Hg at 37 °C. Brains were excised, and one brain hemisphere was fixed in paraformaldehyde followed by 30% sucrose as mentioned previously. Free-floating sections were immunostained with rabbit anti-pimonidazole (1:500) and visualized by Alexa Fluor 488−conjugated goat anti-rabbit secondary antibody (1:1000). The sections were then mounted on dry-gelatin-coated slides and visualized using an EVOS microscope (4× magnification).

2.4.6. Aβ enzyme-linked immunosorbent assay

Protein extraction was prepared by sequential ultracentrifugation of brain subregions homogenates. Frozen tissues of the hippocampus and cortex from 3xTg mice were weighted and mechanically homogenized in ice-cold TBS supplemented with protease inhibitors (P8340; Sigma) and 2 mM EDTA. Samples were ultracentrifuged at 100,000g for 20 minutes at 4 °C, and the collected supernatant was labeled as protein TBS fraction (TBS). Then, the pellet was dissolved to the same volume and homogenized in cold TBS-1% Triton X-100 solution supplemented with protease inhibitors and ultracentrifuged again at 100,000g for 20 minutes at 4 °C. The supernatant was collected and labeled as detergent-soluble fraction (TBSx). The resultant Triton X-100 insoluble pellet was then dissolved to half of the initial homogenization volume in 70% FA and centrifuged at 14,000g for 10 minutes at 4 °C. The supernatant was evaporated off to 70% of the volume with a nitrogen stream and neutralized to pH 7 with 5M

NaOH in 1M Tris. Levels of $A\beta_{1-42}$ and $A\beta_{1-40}$ in the hippocampus and cortex were quantified by β-Amyloid x-42 ELISA Kit (842401; BioLegend) and Aβ x-40 ELISA Kit (842301; BioLegend), respectively. Levels of $A\beta_{1-42}$ and $A\beta_{1-40}$ are presented as picogram/mL of Aβ to total protein mg/mL protein (picogram/mg).

2.4.7. Microglial morphology

WIS-NeuroMath (NeuroMath), a noncommercial automated tracing software from the Weizmann Institute of Science, Rehovot, Israel (Rishal et al., 2013), was used to trace microglia. This tracing method was used to investigate the effects of HBOT on microglial morphology near plaques. Fluorescent images (1024 by 1024 pixels, 8 average) were collected on a Zeiss Meta confocal microscope using a 40× water-immersion objective. Cell somas and branches were detected by NeuroMath and quantified for total process length and total branch points using the NeuroMath's cell measurement output.

2.5. Statistical analysis

Data from behavioral tests, hypoxia analysis, and RT-PCR tests were analyzed by 2-way analysis of variance followed by Fisher least significant difference *post hoc* test. The rest of the data were analyzed by using a Student's unpaired 2-tailed *t* test or Student's unpaired 2-tailed *t* test with Welch's correction (in cases of differences of variances). Data are presented as mean + standard error of the mean. For all analyses, statistical significance was accepted at $p < 0.05$, and trends were defined when $p < 0.10$.

3. Results

3.1. HBOT improves the performance of 3xTg mice in behavioral tasks

To evaluate the effect of HBOT on cognitive performance, 3xTg and non-Tg mice were exposed to HBOT (administration of 100% oxygen at 2 ATA; HBO group) or normobaric air (21% oxygen at 1 ATA; control group) for 60 minutes daily for 14 consecutive days. Following this treatment, mice were subjected to a battery of behavioral tasks. First, spatial recognition memory was investigated by using the mouse's natural preference for exploring novel over familiar spatial contexts in a Y-maze test (Fig. 1A and B). Unlike non-Tg mice, the 3xTg mice did not show any preference for the novel arm and spent similar times in the novel and familiar arms (Fig. 1A; non-Tg-control: 0.63 + 0.02, 3xTg-control: 0.45 + 0.05, $p = 0.0367$). However, the 3xTg mice treated with HBO spent more time in the novel arm than in the familiar one, displaying a significantly higher time index than the untreated 3xTg mice (Fig. 1A and B; 3xTg-HBO: 0.69 + 0.07 vs. 3xTg-control: 0.45 + 0.05, $p = 0.0028$). The frequency index, corresponding to the ratio of the number of entries into the novel arm to the number of entries into novel and familiar arms, was reduced for the untreated 3xTg mice compared with untreated non-Tg mice (Fig. 1B; non-Tg-control: 0.67 + 0.04 vs. 3xTg-control: 0.54 + 0.03, $p = 0.0431$) and was restored for the HBO-treated 3xTg mice (Fig. 1B; 3xTg-HBO: 0.67+ 0.04 vs. 3xTg-control: 0.54+ 0.03, $p = 0.0201$). Next, the mice's locomotor and exploratory activities were tested in an open-field test. In accordance with the literature (Sterniczuk et al., 2010), 3xTg mice showed decreased exploratory behavior as compared to their non-Tg counterparts with shorter walking distance (Fig. 1C; non-Tg-control: 2825 + 208.9 cm vs. 3xTg-control: 1870 + 157.4 cm, $p = 0.0257$) and less entries to the center of the arena (Fig. 1D; non-Tg-control: 63.67 + 10.94 vs. 3xTg-control: 21.77 + 4.369, $p = 0.00075$). However, the exploratory behavior of 3xTg mice was rescued following HBO treatment (Fig. 1C; 3xTg-HBO: 2587 +304.3 cm vs.

3xTg-control: 1870 + 157.4 cm, $p = 0.0240$, Fig. 1D; 3xTg-HBO: 51.78 + 10.04 vs. 3xTg-control: 21.77 ± 4.369, $p = 0.0046$). Finally, the ability to recognize a novel object in an object-recognition test was investigated (Fig. 1E and F). The non-Tg-controls spent more time near the novel object and approached it more than the familiar object, whereas the control 3xTg mice showed no such preference and explored the novel and familiar objects similarly (Fig. 1E; non-Tg-control: 0.69 + 0.05 vs. 3xTg-control: 0.41 + 0.06, $p = 0.0109$ and Fig. 1F; non-Tg-control: 0.61 + 0.05 vs. 3xTg-control: 0.43 + 0.04, $p = 0.0116$). The 3xTg-HBO mice showed improved performance by spending more time next to the novel object compared to the familiar object (Fig. 1E; 3xTg-HBO: 0.63 + 0.06 vs. 3xTg-control: 0.41 + 0.06, $p = 0.0112$) and by approaching it more (Fig. 1F; 3xTg-HBO: 0.59 + 0.04 vs. 3xTg-control: 0.43 + 0.04, $p = 0.0059$). The non-Tg mice treated with HBO did not show any further improvement in behavioral aspects compared with untreated non-Tg mice. Taken together, these results suggest that even in advanced stages of the 3xTg model, HBOT ameliorates their performance in behavioral tasks.

3.2. HBOT reduces amyloid load and tau hyperphosphorylation in 3xTg mice

To assess the effect of HBOT on the amyloid burden in 3xTg mice, brains were stained with the pan-Aβ antibody 4G8 (epitope 17–24; Fig. 2). Previous studies have shown that the 3xTg mouse model displays high amyloid load in the hippocampal formation, localized mainly in the subiculum (Oh et al., 2010). We found a significant reduction in the amyloid burden in the subiculum of the HBO-treated 3xTg mice as manifested in reduced percentage of subiculum area occupied by 4G8 immunoreactivity (64.6%, Fig. 2A and B, $p = 0.0238$ by Welch's correction), number of plaques (40.81%, Fig. 2C, $p = 0.0441$ by Welch's correction), and plaque size (43.2%, Fig. 2D, $p = 0.0128$ by Welch's correction) compared with the untreated 3xTg mice.

To further investigate the effect of HBOT on amyloid pathology in 3xTg mice, hippocampal and cortical lysates were subjected to $A\beta_{1-42}$ and $A\beta_{1-40}$ ELISA analysis (Supplementary data 1A). ELISA analysis revealed that HBOT reduced significantly the levels of $A\beta_{1-42}$ in the TBS-soluble fraction of the hippocampus (Supp. 1A; 54.81%, $p = 0.0486$) and showed only a trend in the insoluble fraction extracted with FA (Supp. 1A; 15.60%, $p = 0.0882$). $A\beta_{1-40}$ levels were not changed by HBOT for all fraction of the hippocampus (Supp. 1B). The ratio of $A\beta_{1-42}/A\beta_{1-40}$ was reduced significantly for triton-soluble fraction (TBSx) of the hippocampus (Supp. 1C; 55.46%, $p = 0.0467$) and showed only a trend for the TBS-soluble fraction (Supp. 1C; 36.49%, $p = 0.0841$). Although $A\beta_{1-42}$ levels were not significantly changed following HBOT in cortical lysates (Supp. 1D), HBOT decreased significantly the levels of $A\beta_{1-40}$ in the TBS-soluble fraction of the cortex (Supp. 1E; 47.20%, $p = 0.0054$). The ratio of $A\beta_{1-42}/A\beta_{1-40}$ was reduced significantly for formic-insoluble fraction (FA) of the cortex (Supp. 1E; reduced by 69.04%, $p = 0.0422$).

The observed changes in Aβ levels can be altered by proteins involved in amyloid precursor protein (APP) processing. Therefore, we investigated whether components of the Aβ-processing pathway could attribute to the observed decrease in amyloid levels in 3xTg mice following HBOT in cortical lysates. Western blot analysis showed that the levels of full-length APP were unaltered with HBO treatment (Fig. 2E and H, $p = 0.1321$). The levels of ADAM10, an α-secretase enzyme, were reduced in 3xTg-HBO-treated mice compared with untreated 3xTg mice (Fig. 2E and H, $p = 0.0098$). The β-secretase-1 levels were also significantly reduced in 3xTg mice following HBOT (Fig. 2F and H, $p = 0.0017$). Presenilin 1, a component of the γ-secretase complex, was

Y-Maze Test
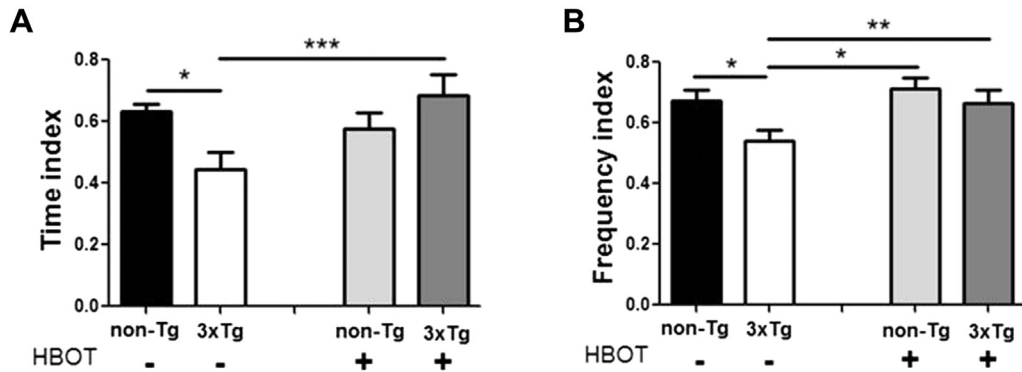
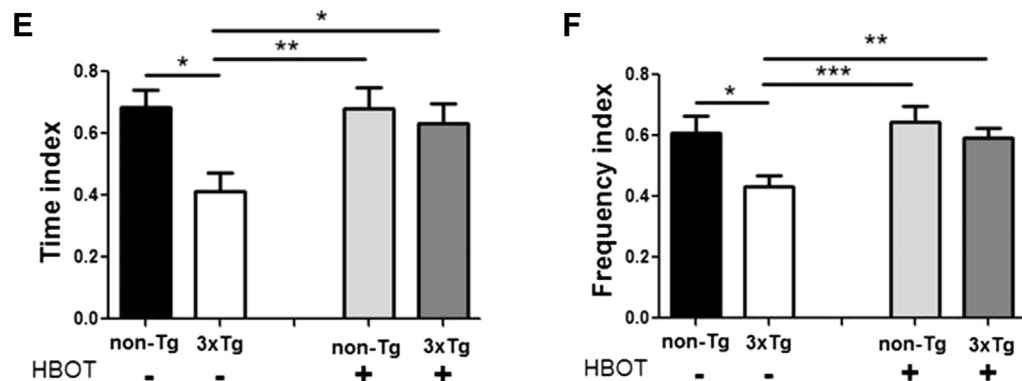# Open-field Test
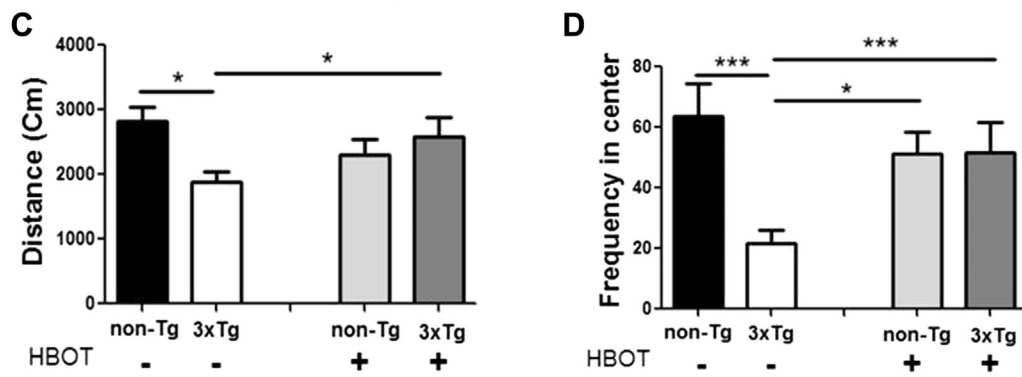
Object Recognition Test

Fig. 1. HBOT improves performance of 3xTg mice in behavioral tasks. (A and B) In the Y-maze test, HBOT restores the preference toward the novel arm in 3xTg mice to non-Tg levels, as demonstrated by the time index (A) and frequency index (B). (C, D) In the open-field test, HBO-treated 3xTg mice show higher locomotion activity than non-treated 3xTg-controls, as demonstrated by distanced traveled (C), and improved spatial navigation as reflected by the number of times the center of the arena was crossed (D). In the object-recognition test, HBO-treated 3xTg mice show higher recognition of the novel object as seen by the time index (E) and the frequency index (F) compared to non-treated 3xTg mice. Values are expressed as mean + SEM. Two-way ANOVA followed by Fisher LSD *post hoc* analysis. Significant differences between groups: $^*p < 0.05$, $^{**}p < 0.01$, $^{***}p < 0.005$; non-Tg (n = 4—6), HBO-treated non-Tg (n = 4—6), 3xTg (*n* = 13—14), and HBO-treated 3xTg (*n* = 9—10). Abbreviations: 3xTg, triple transgenic; ANOVA, analysis of variance; HBOT, hyperbaric oxygen therapy; LSD, least significant difference; SEM, standard error of the mean.

significantly reduced following HBOT (Fig. 2G and H, $p = 0.0220$ by Welch's correction), though no change was found in the levels of other components of the γ-secretase complex, nicastrin (Fig. 2G and H, $p = 0.8599$) and presenilin 2 (Fig. 2G and H, $p = 0.8166$). Taken together, these results suggest that HBOT hampers the abnormal APP processing in 3xTg mice, thus contributing to reduced amyloid pathology in 3xTg mice.

Apart from amyloid plaques, 3xTg mice, expressing the tau[P301L] transgene, also demonstrate progressive tau pathology as they age,

including aggregation of human tau and hyperphosphorylation of tau at several sites (Oddo et al., 2003). To investigate the effect of HBOT on tau pathology in the brains of old 3xTg mice, AT8 immunostaining was performed (Fig. 3A—C). HBO mice displayed a significant decrease in tau phosphorylation at sites Ser202/Thr205 in CA1 (45%, $p = 0.0081$) and subiculum (57.67%, $p = 0.0452$ by Welch's correction) areas. In addition, whereas no change was observed in total tau protein levels with HBOT (TAU5; Fig. 3D and E), tau phosphorylation levels (sites Ser202/Thr205, AT8) were
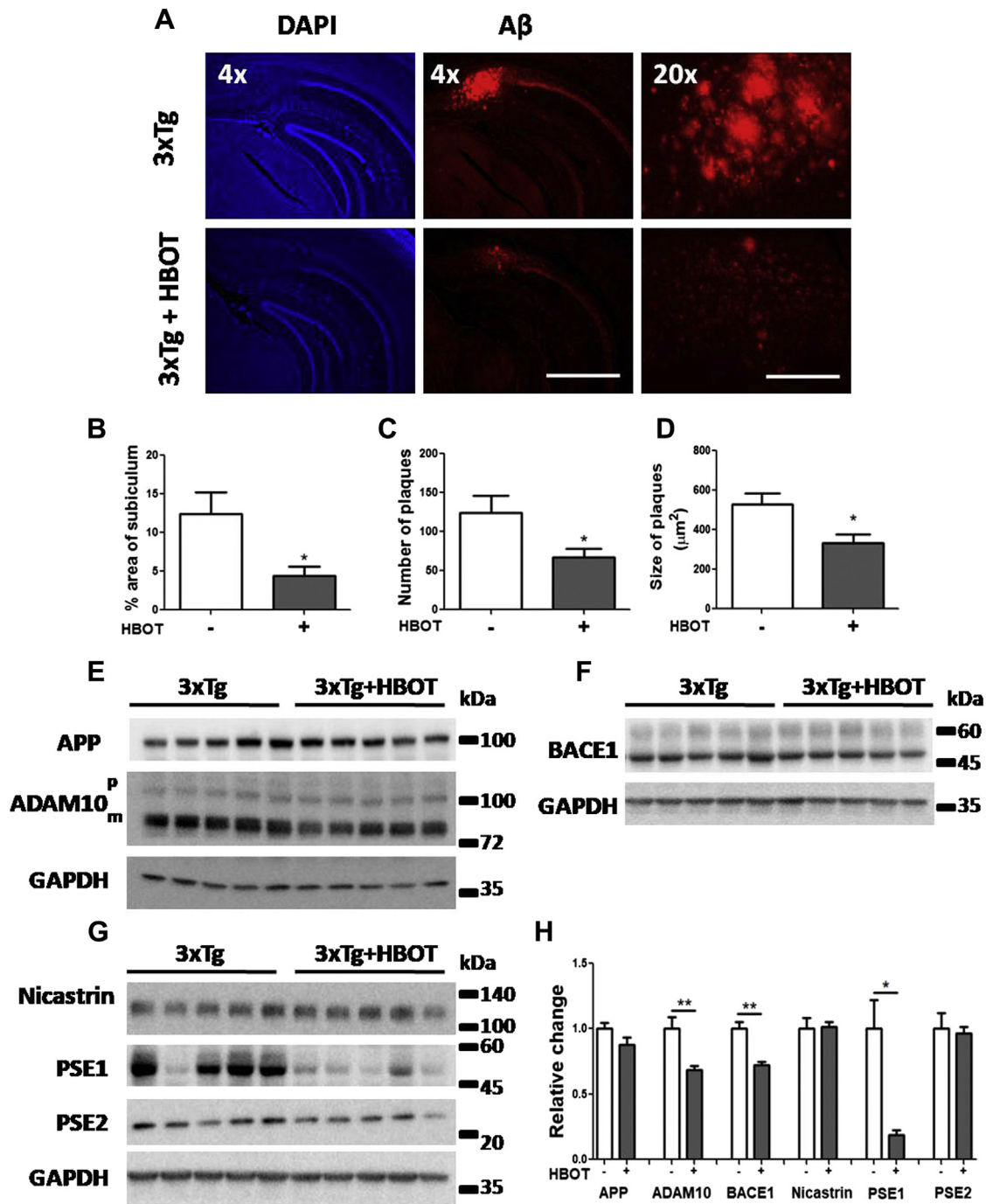
Fig. 2. HBOT reduces amyloid burden in 3xTg mice. Amyloid plaques were visualized by immunostaining with anti-Aβ antibody (4G8). (A) Representative images of Aβ in the hippocampal field of HBO-treated (3xTg+HBOT, n = 9, lower panel) and untreated (3xTg, n = 11, upper panel) 3xTg mice are presented; left and middle panels are 4× magnification, scale bar = 1000 μm; and right panel is 20× magnification, scale bar = 200 μm; DAPI is blue and Aβ is red. (B–D) Quantification of the percentage of subiculum area occupied by plaques (B), the number of plaques (C), and their size (D). (E–G) Representative immunoblot assays of APP processing in the cortex of HBO-treated (n = 5) and untreated 3xTg mice (n = 5). (H) Quantification of the full APP, α-secretase (ADAM10), β-secretase (BACE1), and proteins comprising the γ-secretase complex (Nicastrin, PSE1, and PSE2). Values are expressed as mean + SEM; $^*p < 0.05$, $^{**}p < 0.01$. Abbreviations: 3xTg, triple transgenic; Aβ, β-amyloid; APP, amyloid precursor protein; DAPI, 4′,6-diamidino-2-phenylindole; GAPDH, glyceraldehyde 3-phosphate dehydrogenase; HBOT, hyperbaric oxygen therapy; PSE1, presenilin 1; PSE2, presenilin 2; SEM, standard error of the mean.

significantly reduced in hippocampal lysates from HBO versus control 3xTg mice (48.76%, Fig. 3D and E, $p = 0.0280$). Similarly, tau phosphorylation levels (sites Ser202/Thr205, AT8) were also significantly reduced in cortical lysates from HBO versus control 3xTg mice (82.21%, Fig. 3F and G, $p = 0.0278$ by Welch's correction), while no change was observed in total tau protein levels with HBOT (TAU5; Fig. 3F and G). Next, to elucidate the mechanism through

which HBOT reduces tau phosphorylation in 3xTg mice, we examined the levels of total and a deactivated form of glycogen synthase kinase 3β (GSK3β), a kinase associated with tau phosphorylation in AD (Ferrer et al., 2002; Leroy et al., 2007). We found no change in GSK3β phosphorylation levels at site Ser9, but total GSK3β (tGSKβ) was significantly reduced following HBOT, thus leading to elevated pGSK3β Ser9/tGSK3β ratio, which is associated with reduced
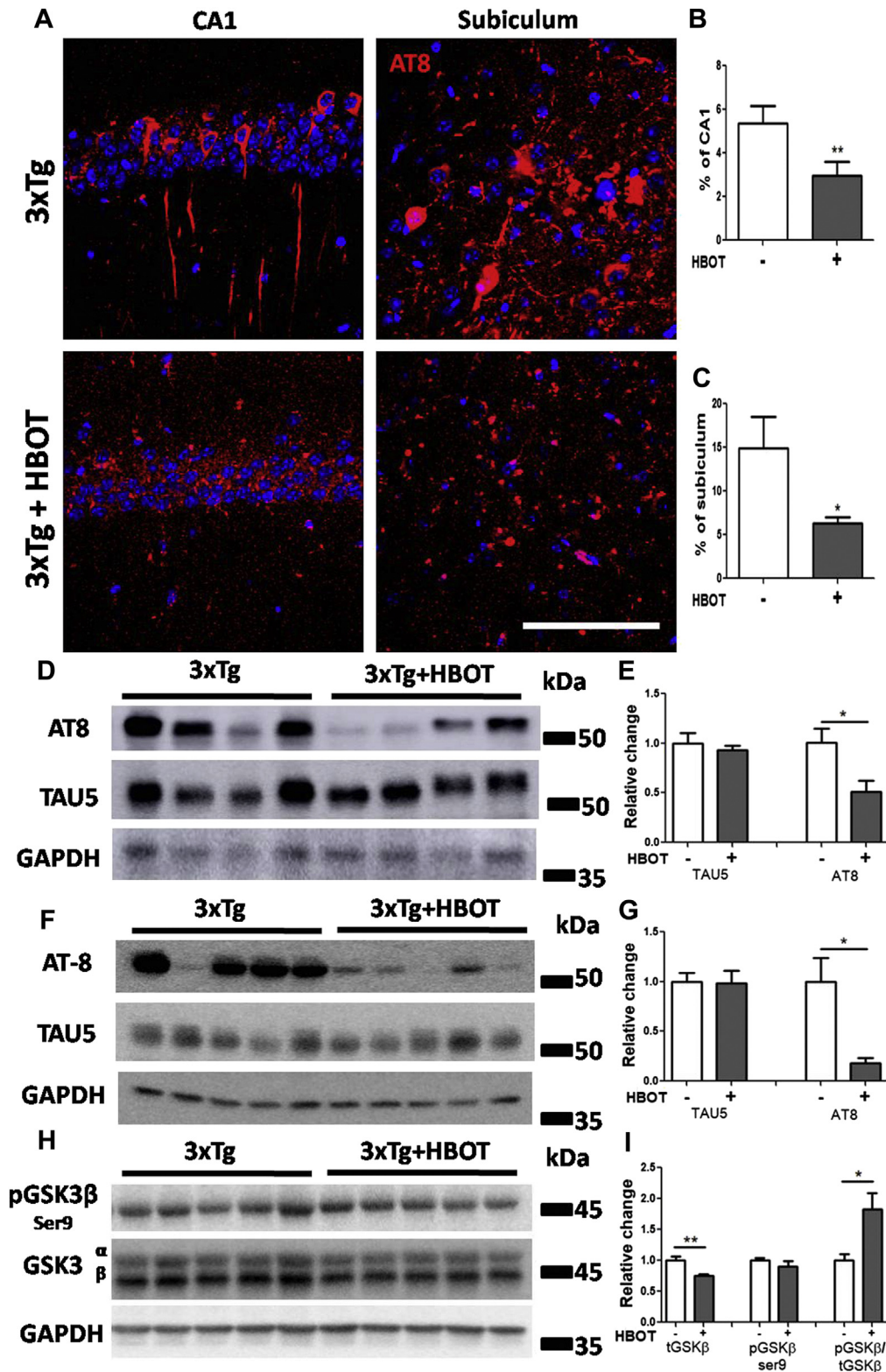
Fig. 3. HBOT ameliorates tau hyperphosphorylation in 3xTg mice. (A) Immunostaining of tau phosphorylation at sites Ser202/Thr205 (AT8; red). Representative images of the CA1 (left panels) and subiculum (right panels) of HBO-treated 3xTg mice (lower panel) and untreated 3xTg mice (upper panel); 40× magnification, scale bar = 50 μm; DAPI is blue. (B and C) Quantification of the percentage of CA1 (B) or subiculum (C) occupied by AT8 immunoreactivity ($n = 10–11$/group). (D–G) Western blots of tau phosphorylation at sites Ser202/Thr205 (AT8) and total tau (TAU5) from hippocampi (D) or cortices (F) extracted from HBO-treated and non-treated 3xTg mice. (E and G) Quantification of Western blots in (D) and (F), respectively, presented as percentage of control, normalized to GAPDH ($n = 4–5$/group). (H) Western blots of total GSK3β (tGSK3β) and phosphorylated GSK3β at site Ser9 from cortices extracted from HBO-treated and non-treated 3xTg mice. (I) Quantification of Western blots in (H), presented as percentage of control, normalized to GAPDH of tGSK3β, pGSK3β and the ratio between pGSK3β and tGSK3β (pGSK3β/tGSK3β) ($n = 5$/group). Values are expressed as mean + SEM; $^*p < 0.05$, $^{**}p < 0.01$. Abbreviations: 3xTg, triple transgenic; DAPI, 4′,6-diamidino-2-phenylindole; GAPDH, glyceraldehyde 3-phosphate dehydrogenase; HBOT, hyperbaric oxygen therapy; SEM, standard error of the mean. (For interpretation of the references to color in this figure legend, the reader is referred to the Web version of this article.)
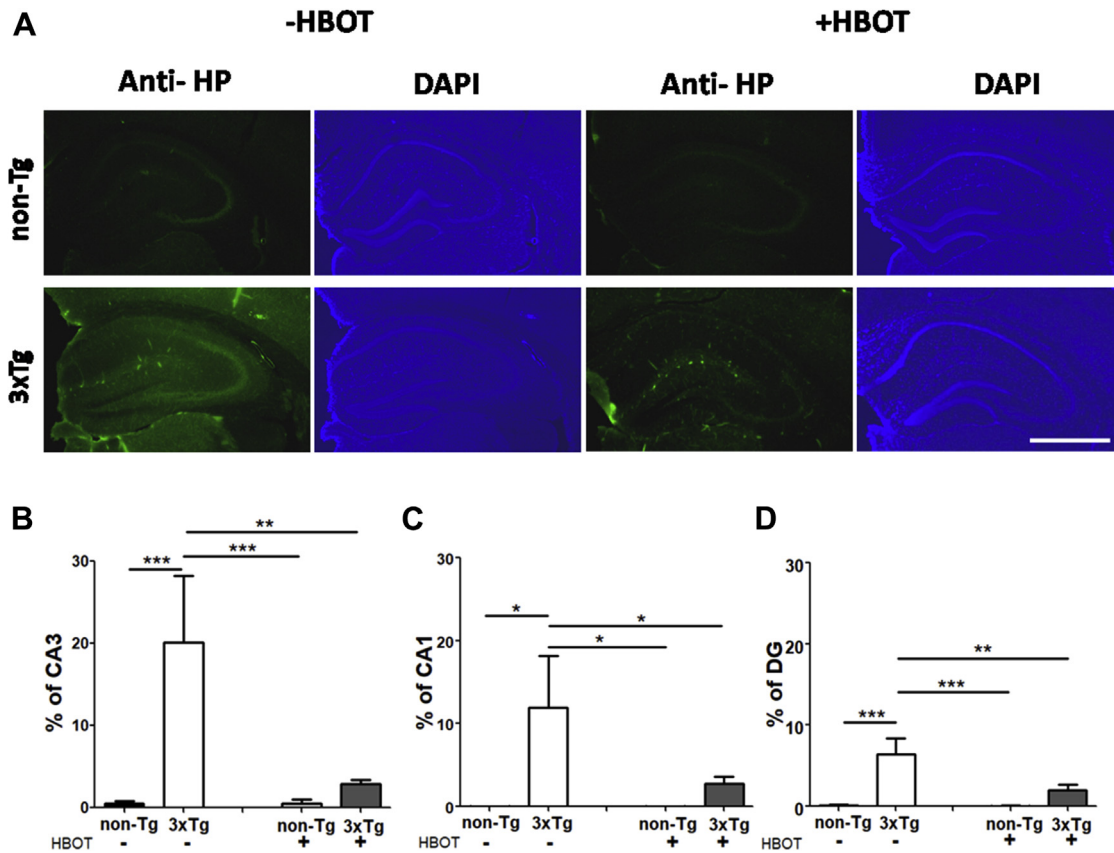
Fig. 4. HBOT reduces the presence of hypoxia in the hippocampal formation of 3xTg mice. Uptake of HP by low-oxygen-bearing cells was visualized using immunofluorescence staining in the hippocampus of HBO-treated and untreated 3xTg and non-Tg mice. (A) Representative images of HP staining in the hippocampal field of HBO-treated (right panels) and untreated (left panels) 3xTg (lower panels) and non-Tg mice (upper panels); 4× magnification, scale bar = 500 μm. (B–D) Quantification of the percentage of HP immunoreactivity occupying the CA3 (B), CA1 (C) and dentate gyrus (DG) (D). Values are expressed as mean + SEM. Two-way ANOVA followed by Fisher LSD *post hoc* analysis. Significant differences between groups: $^*p < 0.05$, $^{**}p < 0.01$, $^{***}p < 0.005$; 3xTg−/+HBOT ($n = 4–5$), non-Tg −/+HBOT (n = 4). Abbreviations: 3xTg, triple transgenic; ANOVA, analysis of variance; DAPI, 4′,6-diamidino-2-phenylindole; HBOT, hyperbaric oxygen therapy; HP, Hypoxyprobe; LSD, least significant difference; SEM, standard error of the mean.

phosphorylation of tau (Cohen and Goedert, 2004). Taken together, our results reveal that HBOT reduces both amyloid and tau pathology and contributes to behavioral recovery in the 3xTg mouse model.

3.3. HBOT reduces the presence of hypoxia in 3xTg mouse hippocampus

Cerebral hypoxia may arise in AD patients due to reduced cerebral perfusion and has been shown to play a crucial role in the pathogenesis of AD (Alsop et al., 2010; Binnewijzend et al., 2013; Chao et al., 2010; Chen et al., 2011; Roher et al., 2012; Thomas et al., 2015; Tosun et al., 2010). The 3xTg mouse model displays hypoperfusion and reduced oxygenation at as early as 8 months of age, thus recapitulating the elements of the hypoxic state seen in patients (Lin et al., 2014). To verify this hypoxic state in old 3xTg mice in comparison with non-Tg, and to determine whether HBOT can revert this condition, Hypoxyprobe staining was conducted. Eight days after the last session of HBO or normobaric treatment, the 3xTg and non-Tg mice were injected with Hypoxyprobe, sacrificed, and their brains were fixed, sectioned and stained with an antibody against Hypoxyprobe. Hypoxyprobe is activated and detectable only in hypoxic cells, which have a partial pressure of oxygen lower than 10 mm Hg (<1%). As can be seen in Fig. 4, the 3xTg-controls showed increased reactivity of Hypoxyprobe compared with their non-Tg controls counterparts in CA3 (40.66-fold increase, $p = 0.0035$), CA1 (325.40-fold increase, $p = 0.0165$),

and dentate gyrus (50.36-fold increase, $p = 0.0006$). Remarkably, HBOT significantly reduced the reactivity of Hypoxyprobe in the hippocampal formation of 3xTg mice, in the CA3 (6.92-fold decrease, $p = 0.0058$), CA1 (5.50-fold decrease, $p = 0.0436$), and the dentate gyrus (4.33-fold decrease, $p = 0.0006$) compared with 3xTg-control mice. These results demonstrate that HBOT reduces the hypoxic state in old 3xTg mice, leading us to explore additional effects of HBOT on AD pathology.

3.4. HBOT reduces astrogliosis in 3xTg mice

As neuroinflammation is one of the hallmarks of AD, and HBOT has been shown to suppress inflammation in both the central nervous system and periphery (Chen et al., 2014; Lavrnja et al., 2015; Lim et al., 2013; Thom, 2011), we examined whether HBOT can also reduce neuroinflammation in the 3xTg mouse model. We first examined the effects of HBOT on astrogliosis near amyloid plaques in the subiculum by double staining for 4G8 and the activated astrocytic marker GFAP (Fig. 5). Confocal images of the subiculum were taken, and the percentage of subiculum area occupied by GFAP immunoreactivity was quantified. HBOT reduced the percentage of subiculum area occupied by GFAP signal by 33.6% (Fig. 5A and B, 10× magnification, $p = 0.0233$) and reduced its immunoreactivity near plaques by 31.8% (Fig. 5C, 40× magnification, $p = 0.0253$ by Welch's correction).
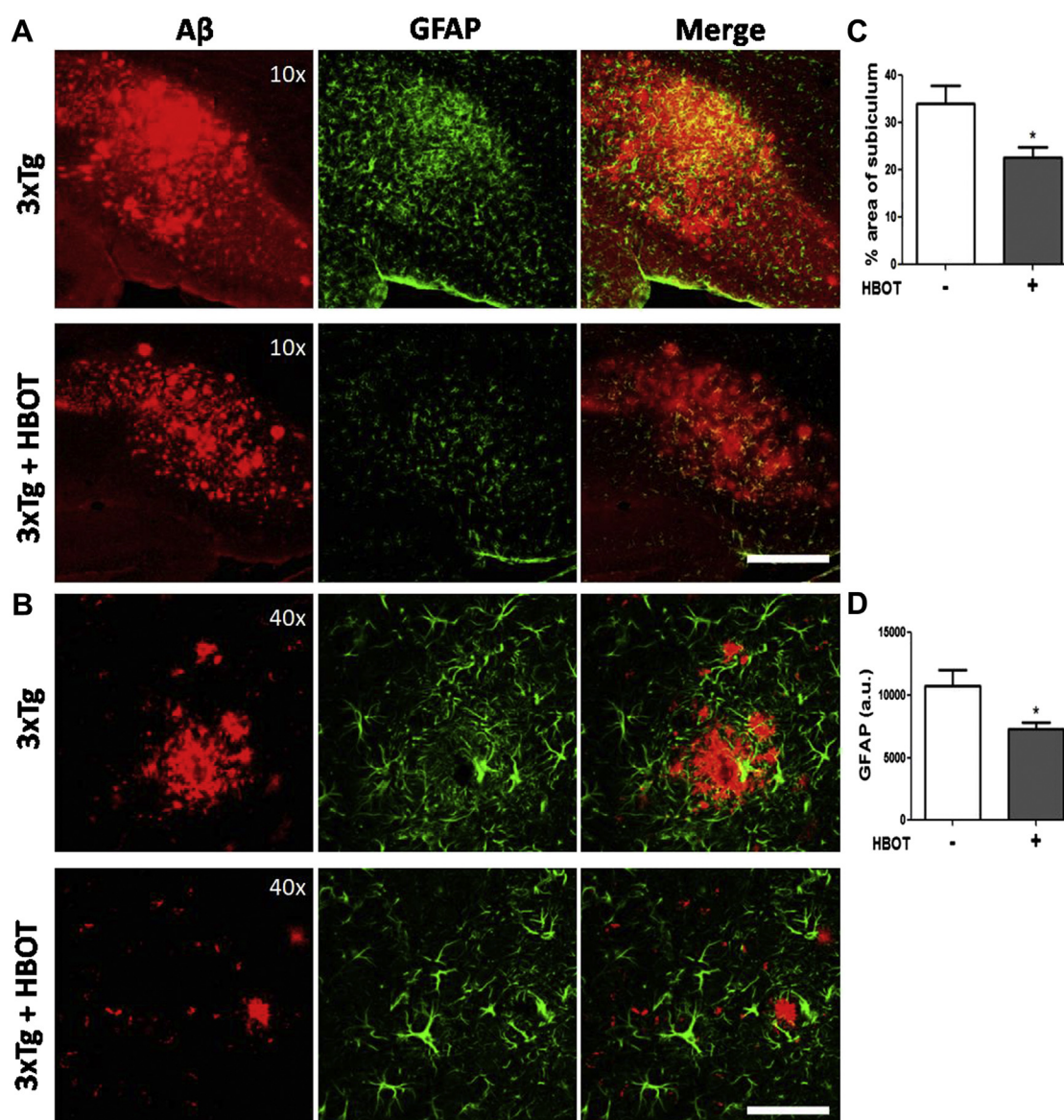
Fig. 5. HBOT reduces astrogliosis in 3xTg mice. (A and B) Immunostaining of Aβ (4G8; red) and activated astrocytes (GFAP; green). Representative images of the subiculum of HBO-treated (lower) and untreated (upper) 3xTg mice; (A) 10× magnification, scale bar = 200 μm and (B) 40× magnification, scale bar = 50 μm. (C) Quantification of the percentage of subiculum occupied by GFAP immunoreactivity and (D) quantification of GFAP immunoreactivity near plaques in the subiculum area. Values are expressed as mean + SEM ($n =$ 9–11/group); $^*p < 0.05$. Abbreviations: 3xTg, triple transgenic; Aβ, β-amyloid; HBOT, hyperbaric oxygen therapy; SEM, standard error of the mean. (For interpretation of the references to color in this figure legend, the reader is referred to the Web version of this article.)

3.5. HBOT reduces the number of microglia near plaques and induces their sprouting

In AD, amyloid depositions are associated with microgliosis, which includes an increase in microglial numbers and their conversion to an activated state. To evaluate the impact of HBOT on microgliosis near amyloid plaques in the subiculum, double staining for 4G8 and the microglial marker Iba1 was conducted (Fig. 6). Confocal images of the subiculum were taken with a 10× objective, and percentage of the subiculum area occupied by Iba1 immunoreactivity was quantified. Iba1 reactivity was reduced in HBO 3xTg mice compared with untreated 3xTg mice (Fig. 5B; $p = 0.0645$).

To more thoroughly investigate the effects of HBOT on microglial numbers and morphology near amyloid plaques in the subiculum area, confocal images were taken with a 40× objective, and their morphology was analyzed with NeuroMath (Galun et al., 2007;

Rishal et al., 2013). HBO-3xTg mice displayed a marked reduction in the number of microglia near plaques (Fig. 6C and D, 36.2%, $p = 0.0130$) and changes in their morphology (Fig. 6C and E). The percentage of sprouting microglial cells near plaques in the HBO mice increased by 17.5% (Fig. 6E, $p = 0.0083$), and their total outgrowth (length of neurites attached to the cells) was enhanced by 27.1% (Table 1, $p = 0.0264$) compared with 3xTg-controls. Microglial process extension, quantified by averaged length over all processes and by length of the cell's longest branch (Table 1), was also enhanced in HBO 3xTg mice. These results demonstrate that HBOT reduces the number of microglia, promotes the elongation of their processes, and increases their branching complexity near plaques. Changes in microglia's morphological characteristics might reflect modifications in their function and activation state, which could lead to increased Aβ clearance and reduced secretion of inflammatory cytokines (Mosher and Wyss-Coray, 2014; Theriault et al., 2015).
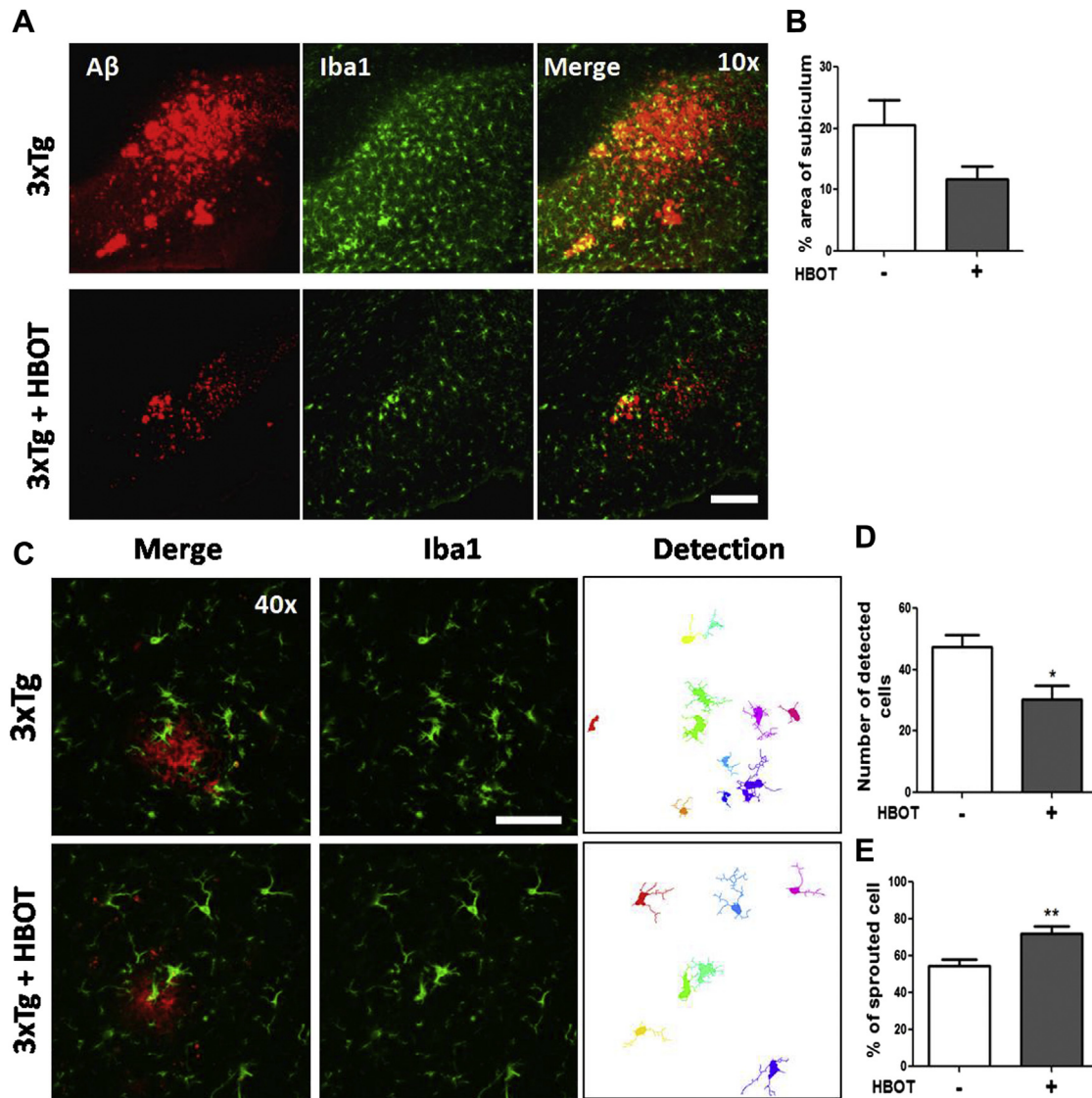
Fig. 6. HBOT reduces the number of microglia near plaques and promotes microglial sprouting. (A) Immunostaining of Aβ (4G8; red) and microglial cells (Iba1; green). Representative images of the subiculum of HBO-treated (lower) and untreated (upper) 3xTg mice; 10× magnification, scale bar = 200 μm. (B) Quantification of the percentage of subiculum occupied by Iba1 immunoreactivity. (C–E) Morphological analysis of individual microglia near amyloid plaques. Confocal images of microglia near plaques in the subiculum area were taken with a 40× objective, and microglial numbers and morphology were analyzed with NeuroMath. (C) Representative images from HBO-treated 3xTg mice (lower panel) and untreated 3xTg mice (upper panel) are displayed on the left, and the detection of individual cells by NeuroMath is displayed on the right; 40× magnification, scale bar = 50 μm. (D) Quantification of the average number of microglial cells near plaques detected by NeuroMath and (E) percentage of sprouting cells out of all detected cells. *$p < 0.05$, **$p < 0.01$. Abbreviations: 3xTg, triple transgenic; Aβ, β-amyloid; HBOT, hyperbaric oxygen therapy. (For interpretation of the references to color in this figure legend, the reader is referred to the Web version of this article.)

3.6. HBOT reduces proinflammatory cytokines and elevates phagocytic markers

As both astrocyte and microglial activation were altered following HBOT, we next investigated whether HBOT changed the cytokine expression and secretion profile, as well as the expression of the phagocytic marker SR-A. Because SR-A (CD204, Scara1, msr1), expressed on microglia, mediates amyloid binding and contributes to its clearance in the brain (El Khoury et al., 1996; Frenkel et al., 2013; Hickman et al., 2008; Koronyo et al., 2015; Paresce et al., 1996), we tested whether HBOT affects this phagocytic marker of microglia. To visualize the expression of SR-A on microglia near amyloid plaques, triple staining for 4G8, Iba1, and SR-A was performed (Fig. 7A–C). Since the number of microglial cells near the

plaques in the HBO mice was significantly reduced, the percentage of Iba1-positive cells expressing SR-A was analyzed. Quantification revealed that the percentage of Iba1-positive cells expressing SR-A was elevated by ∼29% in the HBO mice compared with the controls (Fig. 7C, $p = 0.0004$). This suggested that although HBOT reduces the number of microglia near plaques, it elevates their phagocytic potential, which can play a role in the observed clearance of Aβ (Frenkel et al., 2008). Proinflammatory cytokines such as IL-1β and TNFα are known to contribute to APP processing, tau phosphorylation, and tangle formation, thereby impairing synaptic plasticity, long-term potentiation, and learning and memory processes (Kitazawa et al., 2011; Pickering and O'Connor, 2007; Sheng et al., 2000; Shi et al., 2011; Wang et al., 2005; Yamamoto et al., 2007). TNFα expression is an important component of the

Table 1
HBOT induces microglial sprouting near plaques in the brain of 3xTg mice

Morphological parameter	3xTg (N = 8)	3xTg+ HBOT (N = 10)	*p*-value
Total outgrowth[a]	53.80 ± 4.853	73.81 ± 6.181	0.0264*
Average length over all processes	7.051 ± 0.2509	9.431 ± 0.5901	0.0037**
Length of the cell's longest branch	14.27 ± 0.6551	18.52 ± 1.319	0.0168*
The averaged process length	5.548 ± 0.3141	8.530 ± 0.6512	0.0016**
The averaged longest process length	5.000 ± 0.2632	6.459 ± 0.3290	0.0042**
Maximum over all longest processes	14.27 ± 0.6551	18.52 ± 1.319	0.0168*
Maximum processes length	24.81 ± 2.143	32.93 ± 2.905	0.0475*
N branch points[b]	6.604 ± 0.9092	9.171 ± 0.9986	0.0821#
Branching complexity	0.09241 ± 0.005965	0.1071 ± 0.00387	0.0473*

Quantification of microglial morphology near plaques detected by NeuroMath. Results are presented in micrometers.
Values are expressed as mean + SEM; *$p < 0.05$, **$p < 0.01$, #$p < 0.1$.
[a] Length of processes attached to the cell.
[b] Number of main processes sprouting from cell body.
Key: 3xTg, triple transgenic; HBOT, hyperbaric oxygen therapy; SEM, standard error of the mean.

neuroinflammatory response, and it is strongly expressed in the entorhinal cortex of aged 3xTg mice (Janelsins et al., 2005). We examined TNFα levels in the subiculum of aged 3xTg and found TNFα reactivity to be reduced by 60.28% in the subiculum of 3xTg-HBO mice compared with untreated 3xTg mice (Fig. 7D and E, $p = 0.0088$ by Welch's correction). We also found a reduction in the percentage of astrocytes expressing TNFα in the HBO versus untreated group (∼37.8%, Fig. 7F, $p = 0.0431$).

Finally, we investigated the effect of HBOT on expression of proinflammatory and antiinflammatory cytokines. RNA was extracted from flash-frozen brain tissue of HBO-treated and non-treated 3xTg and non-Tg mice (Fig. 7G), and transcript levels of proinflammatory and antiinflammatory cytokines were measured. The levels of IL-1β, a proinflammatory cytokine, did not change in 3xTg mice compared with non-Tg-controls, yet its levels were significantly reduced in 3xTg mice following HBOT (IL-1β; 1.49-fold decrease, $p = 0.0210$). IL-4, an antiinflammatory cytokine, did not change as well in 3xTg mice compared with non-Tg-controls, but HBOT elevated its levels by 2.27-fold in 3xTg mice (*IL-4*; $p = 0.00005$). Notably, IL-4 was also elevated in non-Tg mice following HBOT (*IL-4*; $p = 0.0128$). IL-10, another antiinflammatory cytokine, was reduced significantly in 3xTg mice compared with non-Tg mice (IL-10; 2.52-fold decrease, $p = 0.0178$) and was ameliorated in HBO-treated 3xTg mice to non-Tg levels (IL-10; 2.58-fold increase, $p = 0.0143$). The expressions of arginase1 (*arg1*) and SR-A (*Msr1*), markers for phagocytic activation (Medeiros et al., 2013), were both significantly reduced in 3xTg-controls compared with non-Tg-controls (*arg1*; 5.02-fold reduction, $p = 0.000004$ and *msr1*; 2.10-fold reduction, $p = 0.0449$), suggesting microglia phagocytic activity is severely impaired in old 3xTg mice. HBOT increased arginase1 levels by 1.84-fold in 3xTg mice (statistically significant; $p = 0.0182$ by Welch's correction). However, when this effect was tested with non-Tg mice (2-way analysis of variance), it did not reach significance because of a strong genotype effect (*arg1*; 1.84-fold reduction, $p = 0.2090$). Interestingly, the transcript levels of SR-A in HBO-treated 3xTg mice were restored back to non-Tg levels (*Msr1*; 2.30-fold change, $p = 0.0150$) (Fig. 7G). The latter finding is in agreement with the increased levels of SR-A reactivity on the microglia (Fig. 7A–C) and suggests that HBOT increases phagocytosis of Aβ. Together with the observed HBOT suppression of astrogliosis and microgliosis, these data suggest that HBOT reduces neuroinflammation, improves antiinflammatory processes, and elevates phagocytic markers even in old AD mice.

4. Discussion

HBOT has potent neuroprotective effects in patients and animal models of hypoxia-related neurological diseases (Boussi-Gross et al., 2015; Figueroa and Wright, 2015; Hadanny et al., 2015; Huang and Obenaus, 2011; Tal et al., 2015). In this study, for the first time, the effects of HBOT on amyloid deposition, tau pathology, neuroinflammation, and additional pathologies were investigated in the 3xTg mouse model of AD. The results of the present study revealed that HBOT reduces brain hypoxia, amyloid burden, and tau phosphorylation and attenuates neuroinflammation. The reduced amyloid pathology in 3xTg mice was associated with attenuation in the abnormal APP processing, whereas the reduction of tau hyperphosphorylation was associated with elevated pGSK3β/tGSK3β ratio. These changes were accompanied with reduction in proinflammatory cytokines, elevation in antiinflammatory cytokines and phagocytic markers, and improvement in behavioral deficits in old 3xTg mice.

Growing evidence suggests that AD patients present reduced cerebral perfusion, which can be detected in early stages of the disease and deteriorates with disease progression (Alsop et al., 2010; Binnewijzend et al., 2013; Chao et al., 2010; Chen et al., 2011; Roher et al., 2012; Thomas et al., 2015; Tosun et al., 2010). Moreover, hypoxia has been shown to contribute to several AD pathologies, such as accumulation of Aβ, hyperphosphorylation of tau, neuroinflammation, and degeneration of neurons (Zhang and Le, 2010). In agreement with Lin et al.'s report (Lin et al., 2014) of decreased cerebral oxygen concentration in the 3xTg-AD model, we detected hypoxia in the hippocampus of 17-month-old 3xTg mice. Therefore, the 3xTg-AD model is relevant for studying the effects of HBOT as it not only successfully mimics this aspect of the human disease but also presents amyloid and tau pathologies, increased inflammation, and deficits in behavioral tests.

One of the primary and immediate mechanisms of HBOT is enhancement of arterial partial pressure of oxygen and oxygen content in compromised tissue (Gill and Bell, 2004; Thom, 2011). Accordingly, HBOT reduced the presence of hypoxia in the hippocampus of aged 3xTg mice. Interestingly, the reduced hypoxia was observed 8 days after the last treatment, suggesting that this effect lasts for some time after the last HBOT session. This effect might be attributed to improved cerebral vascular flow due to HBOT-induced vascular remodeling or angiogenesis (Camporesi and Bosco, 2014; Duan et al., 2015; Lin et al., 2012; Tal et al., 2015).

Recently, it was shown that a mild elevation of oxygen (from 21% to 32%) results in improved cognitive performance and upregulation of proteins involved in the clearance of Aβ in the eye lenses of 3xTg mice (Wang et al., 2016). HBOT increases tissue oxygenation more effectively than simple oxygen supplementation (Calvert et al., 2007; Meirovithz et al., 2007; Tibbles and Edelsberg, 1996; van Hulst et al., 2003) and indeed, our results showed that HBOT improves amyloid clearance and performance in behavioral tasks,
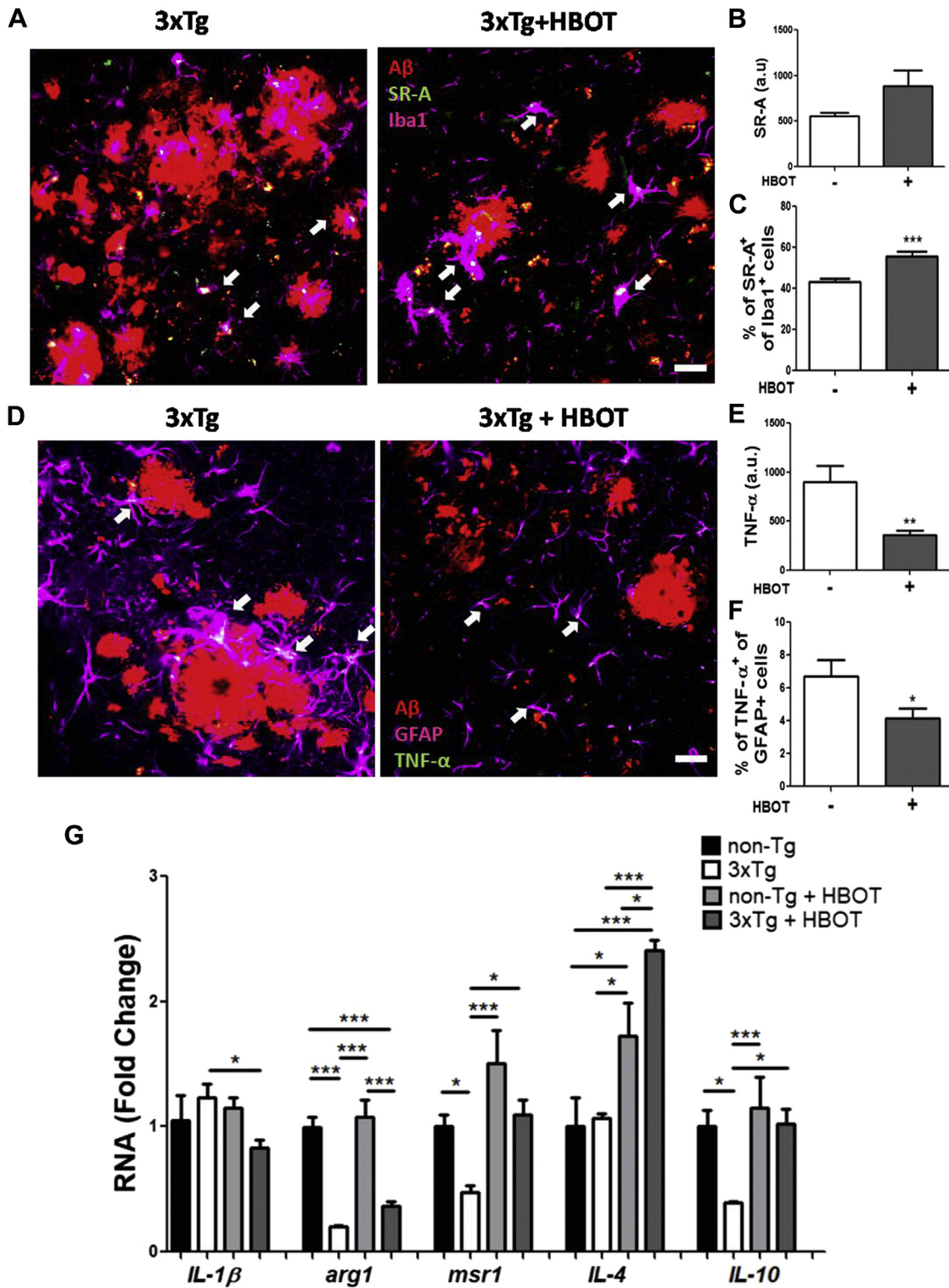
Fig. 7. HBOT reduces proinflammatory cytokines and increases antiinflammatory cytokines and phagocytic markers. (A−C) Immunostaining of Aβ (4G8; red), activated astrocytes (GFAP; pink), and SR-A (CD204; green). (A) Representative images of the subiculum of HBO-treated (right) and untreated (left) 3xTg mice; 40× magnification, scale bar = 50 μm. White arrows indicate examples of Iba1+ and CD204+ cells. (B) Quantification of CD204 immunoreactivity and (C) percentage of Iba1+ cells expressing CD204. (D−F) Immunostaining of Aβ (4G8; red), astrocytes (GFAP; pink) and TNFα (green). Representative images of the subiculum of HBO-treated (right) and untreated (left) 3xTg mice; 40× magnification, scale bar = 50 μm. White arrows indicate examples of cells expressing GFAP and TNFα immunoreactivity (D). Quantification of TNFα immunoreactivity (E) and percentage of GFAP-positive cells expressing TNFα near plaques in the subiculum area (F). Values are expressed as mean + SEM ($n = 8−11$/group); $^*p < 0.05$, $^{**}p < 0.01$. (G) RNA transcripts for inflammation-related genes extracted from hippocampal tissue of HBO-treated and untreated 3xTg and non-Tg mice were analyzed using TaqMan real-time quantitative PCR assays. Values are expressed as mean + SEM ($n = 4−5$/group). Two-way ANOVA followed by Fisher LSD *post hoc* analysis. Significant differences between groups: $^*p < 0.05$, $^{**}p < 0.01$, $^{***}p < 0.005$. Abbreviations: 3xTg, triple transgenic; Aβ, β-amyloid; ANOVA, analysis of variance; HBOT, hyperbaric oxygen therapy; LSD, least significant difference; SEM, standard error of the mean; TNFα, tumor necrosis factor alpha. (For interpretation of the references to color in this figure legend, the reader is referred to the Web version of this article.)

suggesting that oxygen is a rate-limiting factor for tissue recovery in AD.

Neuroinflammation plays a crucial role in AD. In specimens of Alzheimer patients, the activation and accumulation of microglia and astrocytes around Aβ plaques have long been described (Itagaki et al., 1989; Terry et al., 1964; Wisniewski et al., 1989). In early stages of the disease, microglial activation in an M2-like phenotype has neuroprotective effects by preventing plaque formation and promoting removal of existing Aβ deposits. However, in later stages of the disease, sustained exposure to Aβ, neuronal debris, and proinflammatory cytokines mediates a switch to a detrimental M1-like phenotype characterized by increased proinflammatory secretion, reduced phagocytosis, and a "reactive" morphology, with short, thick, and poorly ramified processes (Mosher and Wyss-Coray, 2014). This detrimental activation state can be reverted by a variety of treatments (Daniels et al., 2016; McGeer and McGeer, 2015). In the present study, we demonstrated that HBOT reduces microgliosis, astrogliosis, and the secretion of proinflammatory cytokines, such as IL-1β and TNFα, and increased the production of antiinflammatory cytokines, such as IL-4 and IL-10. Furthermore, HBOT induced a morphological change in microglia near plaques to a more ramified state and increased microglial expression of SR-A, which is known to mediate Aβ clearance (El Khoury et al., 1996; Frenkel et al., 2013; Koronyo et al., 2015; Paresce et al., 1996) and arginase1, which has been shown to be expressed by microglia involved in Aβ plaque reduction during sustained neuroinflammation (Cherry et al., 2015). It should be noted that although HBOT increased both arginase1 and SR-A levels in 3xTg mice following HBOT, SR-A was restored to non-Tg levels while arginase1 was elevated but did not reach control non-Tg levels, suggesting differential effects of HBOT on phagocytic markers. Furthermore, these changes were associated with a striking decrease in amyloid load and tau phosphorylation. Taken together, we suggest that HBOT shifts microglial function from the M1-like to M2-like phenotype, enabling their neuroprotective function and an increased Aβ clearance (Heneka et al., 2013).

It has recently been shown that elimination of microglia in murine models of AD at advanced stages reduces overall neuroinflammation and improves contextual memory without altering amyloid levels (Dagher et al., 2015; Grathwohl et al., 2009; Spangenberg et al., 2016). Similarly, targeting of TNFα also resulted in attenuation of behavioral deficits in animal models of AD (McAlpine et al., 2009; Tweedie et al., 2012) and improvement in cognitive measurements of patients with mild-to-severe AD (Tobinick et al., 2006). Our results show that HBOT reduces the number of microglia and reduces neuroinflammation while improving behavioral tasks. Based on these results, targeting neuroinflammation may hold the key for developing disease-modifying treatments for AD, even at late stages of the disease.

The HBOT-induced modulation of the immune system demonstrated here is consistent with previous studies investigating the effect of HBOT on other neurological conditions such as traumatic brain injury (Chen et al., 2014; Geng et al., 2016; Lavrnja et al., 2015; Lim et al., 2013), stroke and ischemia (Gunther et al., 2005; Yang et al., 2015), and spinal cord injury (Geng et al., 2016; Yu et al., 2004). Specifically, IL-10, an antiinflammatory cytokine, has been reported to be elevated following HBOT in other neurological condition (Chen et al., 2014). In accordance, we found that HBOT restored IL-10 levels in 3xTg mice back to non-Tg levels. Moreover, we detected that IL-4, another antiinflammatory cytokine, was significantly elevated following HBOT in both 3xTg and non-Tg mice, suggesting HBOT exerts its beneficial effects by differentially modulating the immune system in neurological conditions.

For many years, the main concern with using HBOT for the treatment of neurological conditions, and specifically AD, was elevation of reactive oxygen species and augmentation of oxidative stress, which is thought to increase susceptibility to disease progression. However, evidence suggests that although HBOT increases the level of lipid peroxidation and/or protein oxidation in blood and tissues of HBO-exposed organisms, it significantly elevates scavenging antioxidants (such as superoxide dismutase, catalase, and glutathione peroxidase) and thus reduces oxidative damage to the tissue (Simsek et al., 2012). In fact, some reports argue that reactive oxygen species generation under HBOT conditions mediates some of its beneficial effects (Simsek et al., 2015; Thom, 2009). In AD models, it has been shown that elevation of oxygen in the brain by simple oxygen supplementation (Wang et al., 2016) or HBOT (Tian et al., 2012, 2013) increases the activity and/or number of antioxidant enzymes and leads to suppression of oxidative damage and decreased neuronal degeneration. Therefore, it seems that although HBOT increases oxygen levels in the brain, it also significantly activates the antioxidant pathways and should therefore also be tolerable and safe for the treatment of AD. Moreover, growing evidence suggests that HBOT can induce neuroplasticity and improve cognitive function in patients suffering from chronic neurocognitive impairment due to stroke, traumatic brain injuries, and anoxic brain damage (Boussi-Gross et al., 2015; Efrati et al., 2013; Tal et al., 2015). This information, together with the fundamental data acquired by this work, gives insights into upcoming clinical studies of HBOT for patients suffering from AD.

Here, we show for the first time that HBOT can ameliorate AD pathology and behavioral deficits in a transgenic mouse model of AD. HBOT is a well-tolerated and safe treatment that is used in the clinic for various medical conditions (Hadanny et al., 2016; Tibbles and Edelsberg, 1996), including neurological disorders. Although further research is needed to elucidate the underlying beneficial mechanisms of HBOT and to evaluate its beneficial effects in various Alzheimer patient populations, we suggest that HBOT presents a new platform for the treatment of AD.

Acknowledgements

Appendix A. Supplementary data

Supplementary data associated with this article can be found, in the online version, at https://doi.org/10.1016/j.neurobiolaging.2017.10.007.

References

Alsop, D.C., Dai, W., Grossman, M., Detre, J.A., 2010. Arterial spin labeling blood flow MRI: its role in the early characterization of Alzheimer's disease. J. Alzheimer's Dis. 20 (3), 871–880.

Altieri, M., Di Piero, V., Pasquini, M., Gasparini, M., Vanacore, N., Vicenzini, E., Lenzi, G.L., 2004. Delayed poststroke dementia: a 4-year follow-up study. Neurology 62, 2193–2197.

Binnewijzend, M.A., Kuijer, J.P., Benedictus, M.R., van der Flier, W.M., Wink, A.M., Wattjes, M.P., van Berckel, B.N., Scheltens, P., Barkhof, F., 2013. Cerebral blood flow measured with 3D pseudocontinuous arterial spin-labeling MR imaging in Alzheimer disease and mild cognitive impairment: a marker for disease severity. Radiology 267, 221–230.

Boussi-Gross, R., Golan, H., Volkov, O., Bechor, Y., Hoofien, D., Beeri, M.S., Ben-Jacob, E., Efrati, S., 2015. Improvement of memory impairments in poststroke patients by hyperbaric oxygen therapy. Neuropsychology 29, 610–621.

Braak, H., Braak, E., 1997. Staging of Alzheimer-related cortical destruction. Int. Psychogeriatr 1, 257—261.

Calvert, J.W., Cahill, J., Zhang, J.H., 2007. Hyperbaric oxygen and cerebral physiology. Neurol. Res. 29, 132—141.

Camporesi, E.M., Bosco, G., 2014. Mechanisms of action of hyperbaric oxygen therapy. Undersea Hyperb. Med. 41, 247—252.

Chao, L.L., Buckley, S.T., Kornak, J., Schuff, N., Madison, C., Yaffe, K., Miller, B.L., Kramer, J.H., Weiner, M.W., 2010. ASL perfusion MRI predicts cognitive decline and conversion from MCI to dementia. Alzheimer Dis. Assoc. Disord. 24, 19—27.

Chen, J.J., Rosas, H.D., Salat, D.H., 2011. Age-associated reductions in cerebral blood flow are independent from regional atrophy. Neuroimage 55, 468—478.

Chen, X., Duan, X.S., Xu, L.J., Zhao, J.J., She, Z.F., Chen, W.W., Zheng, Z.J., Jiang, G.D., 2014. Interleukin-10 mediates the neuroprotection of hyperbaric oxygen therapy against traumatic brain injury in mice. Neuroscience 266, 235—243.

Cherry, J.D., Olschowka, J.A., O'Banion, M.K., 2015. Arginase 1+ microglia reduce Aβ plaque deposition during IL-1β-dependent neuroinflammation. J. Neuroinflammation 12, 203.

Cohen, P., Goedert, M., 2004. GSK3 inhibitors: development and therapeutic potential. Nat. Rev. Drug Discov. 3, 479—487.

Dagher, N.N., Najafi, A.R., Kayala, K.M., Elmore, M.R., White, T.E., Medeiros, R., West, B.L., Green, K.N., 2015. Colony-stimulating factor 1 receptor inhibition prevents microglial plaque association and improves cognition in 3xTg-AD mice. J. Neuroinflammation 12, 015—0366.

Daniels, M.J., Rivers-Auty, J., Schilling, T., Spencer, N.G., Watremez, W., Fasolino, V., Booth, S.J., White, C.S., Baldwin, A.G., Freeman, S., Wong, R., Latta, C., Yu, S., Jackson, J., Fischer, N., Koziel, V., Pillot, T., Bagnall, J., Allan, S.M., Paszek, P., Galea, J., Harte, M.K., Eder, C., Lawrence, C.B., Brough, D., 2016. Fenamate NSAIDs inhibit the NLRP3 inflammasome and protect against Alzheimer's disease in rodent models. Nat. Commun. 7, 12504.

Duan, S., Shao, G., Yu, L., Ren, C., 2015. Angiogenesis contributes to the neuroprotection induced by hyperbaric oxygen preconditioning against focal cerebral ischemia in rats. Int. J. Neurosci. 125, 625—634.

Efrati, S., Fishlev, G., Bechor, Y., Volkov, O., Bergan, J., Kliakhandler, K., Kamiager, I., Gal, N., Friedman, M., Ben-Jacob, E., Golan, H., 2013. Hyperbaric oxygen induces late neuroplasticity in post stroke patients—randomized, prospective trial. PLoS One 8, 15.

El Khoury, J., Hickman, S.E., Thomas, C.A., Cao, L., Silverstein, S.C., Loike, J.D., 1996. Scavenger receptor-mediated adhesion of microglia to beta-amyloid fibrils. Nature 382, 716—719.

Ferrer, I., Barrachina, M., Puig, B., 2002. Glycogen synthase kinase-3 is associated with neuronal and glial hyperphosphorylated tau deposits in Alzheimer's disease, Pick's disease, progressive supranuclear palsy and corticobasal degeneration. Acta Neuropathol. 104, 583—591.

Figueroa, X.A., Wright, J.K., 2015. Clinical results in brain injury trials using HBO2 therapy: another perspective. Undersea Hyperb. Med. 42, 333—351.

Frenkel, D., Puckett, L., Petrovic, S., Xia, W., Chen, G., Vega, J., Dembinsky-Vaknin, A., Shen, J., Plante, M., Burt, D.S., Weiner, H.L., 2008. A nasal proteosome adjuvant activates microglia and prevents amyloid deposition. Ann. Neurol. 63, 591—601.

Frenkel, D., Wilkinson, K., Zhao, L., Hickman, S.E., Means, T.K., Puckett, L., Farfara, D., Kingery, N.D., Weiner, H.L., El Khoury, J., 2013. Scara1 deficiency impairs clearance of soluble amyloid-beta by mononuclear phagocytes and accelerates Alzheimer's-like disease progression. Nat. Commun. 4.

Galun, M., Basri, R., Brandt, A., 2007. Multiscale edge detection and fiber enhancement using differences of oriented means. IEEE Conf. Comp. Vis. 722—729.

Geng, F., Ma, Y., Xing, T., Zhuang, X., Zhu, J., Yao, L., 2016. Effects of hyperbaric oxygen therapy on inflammasome signaling after traumatic brain injury. Neuroimmunomodulation 23, 122—129.

Gill, A.L., Bell, C.N., 2004. Hyperbaric oxygen: its uses, mechanisms of action and outcomes. Qjm 97, 385—395.

Grathwohl, S.A., Kalin, R.E., Bolmont, T., Prokop, S., Winkelmann, G., Kaeser, S.A., Odenthal, J., Radde, R., Eldh, T., Gandy, S., Aguzzi, A., Staufenbiel, M., Mathews, P.M., Wolburg, H., Heppner, F.L., Jucker, M., 2009. Formation and maintenance of Alzheimer's disease beta-amyloid plaques in the absence of microglia. Nat. Neurosci. 12, 1361—1363.

Gunther, A., Kuppers-Tiedt, L., Schneider, P.M., Kunert, I., Berrouschot, J., Schneider, D., Rossner, S., 2005. Reduced infarct volume and differential effects on glial cell activation after hyperbaric oxygen treatment in rat permanent focal cerebral ischaemia. Eur. J. Neurosci. 21, 3189—3194.

Hadanny, A., Golan, H., Fishlev, G., Bechor, Y., Volkov, O., Suzin, G., Ben-Jacob, E., Efrati, S., 2015. Hyperbaric oxygen can induce neuroplasticity and improve cognitive functions of patients suffering from anoxic brain damage. Restor Neurol. Neurosci. 33, 471—486.

Hadanny, A., Meir, O., Bechor, Y., Fishlev, G., Bergan, J., Efrati, S., 2016. Seizures during hyperbaric oxygen therapy: retrospective analysis of 62,614 treatment sessions. Undersea Hyperb. Med. 43, 21—28.

Harch, P.G., 2015. Hyperbaric oxygen in chronic traumatic brain injury: oxygen, pressure, and gene therapy. Med. Gas Res. 5, 015—0030.

Heinonen, O., Soininen, H., Sorvari, H., Kosunen, O., Paljarvi, L., Koivisto, E., Riekkinen Sr., P.J., 1995. Loss of synaptophysin-like immunoreactivity in the hippocampal formation is an early phenomenon in Alzheimer's disease. Neuroscience 64, 375—384.

Heneka, M.T., Kummer, M.P., Stutz, A., Delekate, A., Schwartz, S., Vieira-Saecker, A., Griep, A., Axt, D., Remus, A., Tzeng, T.C., Gelpi, E., Halle, A., Korte, M., Latz, E., Golenbock, D.T., 2013. NLRP3 is activated in Alzheimer's disease and contributes to pathology in APP/PS1 mice. Nature 493, 674—678.

Hickman, S.E., Allison, E.K., El Khoury, J., 2008. Microglial dysfunction and defective beta-amyloid clearance pathways in aging Alzheimer's disease mice. J. Neurosci. 28, 8354—8360.

Honig, L.S., Kukull, W., Mayeux, R., 2005. Atherosclerosis and AD: analysis of data from the US National Alzheimer's Coordinating Center. Neurology 64, 494—500.

Hoozemans, J.J., Veerhuis, R., Rozemuller, J.M., Eikelenboom, P., 2006. Neuroinflammation and regeneration in the early stages of Alzheimer's disease pathology. Int. J. Dev. Neurosci. 24, 157—165.

Huang, L., Obenaus, A., 2011. Hyperbaric oxygen therapy for traumatic brain injury. Med. Gas Res. 1, 2045—9912.

Iram, T., Trudler, D., Kain, D., Kanner, S., Galron, R., Vassar, R., Barzilai, A., Blinder, P., Fishelson, Z., Frenkel, D., 2016. Astrocytes from old Alzheimer's disease mice are impaired in Abeta uptake and in neuroprotection. Neurobiol. Dis. 96, 84—94.

Itagaki, S., McGeer, P.L., Akiyama, H., Zhu, S., Selkoe, D., 1989. Relationship of microglia and astrocytes to amyloid deposits of Alzheimer disease. J. Neuroimmunol 24, 173—182.

Janelsins, M.C., Mastrangelo, M.A., Oddo, S., LaFerla, F.M., Federoff, H.J., Bowers, W.J., 2005. Early correlation of microglial activation with enhanced tumor necrosis factor-alpha and monocyte chemoattractant protein-1 expression specifically within the entorhinal cortex of triple transgenic Alzheimer's disease mice. J. Neuroinflammation 2, 23.

Jellinger, K.A., Bancher, C., 1996. AD neuropathology. Neurology 46, 1186—1187.

Kaur, C., Rathnasamy, G., Ling, E.A., 2013. Roles of activated microglia in hypoxia induced neuroinflammation in the developing brain and the retina. J. Neuroimmune Pharmacol. 8, 66—78.

Kitazawa, M., Cheng, D., Tsukamoto, M.R., Koike, M.A., Wes, P.D., Vasilevko, V., Cribbs, D.H., LaFerla, F.M., 2011. Blocking IL-1 signaling rescues cognition, attenuates tau pathology, and restores neuronal beta-catenin pathway function in an Alzheimer's disease model. J. Immunol. 187, 6539—6549.

Koronyo, Y., Salumbides, B.C., Sheyn, J., Pelissier, L., Li, S., Ljubimov, V., Moyseyev, M., Daley, D., Fuchs, D.T., Pham, M., Black, K.L., Rentsendorj, A., Koronyo-Hamaoui, M., 2015. Therapeutic effects of glatiramer acetate and grafted CD115(+) monocytes in a mouse model of Alzheimer's disease. Brain 138 (Pt 8), 2399—2422.

Lai, A.Y., Todd, K.G., 2006. Hypoxia-activated microglial mediators of neuronal survival are differentially regulated by tetracyclines. Glia 53, 809—816.

Lavrnja, I., Parabucki, A., Brkic, P., Jovanovic, T., Dacic, S., Savic, D., Pantic, I., Stojiljkovic, M., Pekovic, S., 2015. Repetitive hyperbaric oxygenation attenuates reactive astrogliosis and suppresses expression of inflammatory mediators in the rat model of brain injury. Mediators Inflamm. 2015, 498405.

Leroy, K., Yilmaz, Z., Brion, J.P., 2007. Increased level of active GSK-3β in Alzheimer's disease and accumulation in argyrophilic grains and in neurones at different stages of neurofibrillary degeneration. Neuropathol. Appl. Neurobiol. 33, 43—55.

Lim, S.W., Wang, C.C., Wang, Y.H., Chio, C.C., Niu, K.C., Kuo, J.R., 2013. Microglial activation induced by traumatic brain injury is suppressed by postinjury treatment with hyperbaric oxygen therapy. J. Surg. Res. 184, 1076—1084.

Lin, J.W., Tsai, J.T., Lee, L.M., Lin, C.M., Hung, C.C., Hung, K.S., Chen, W.Y., Wei, L., Ko, C.P., Su, Y.K., Chiu, W.T., 2008. Effect of hyperbaric oxygen on patients with traumatic brain injury. Acta Neurochir Suppl. 101, 145—149.

Lin, K.C., Niu, K.C., Tsai, K.J., Kuo, J.R., Wang, L.C., Chio, C.C., Chang, C.P., 2012. Attenuating inflammation but stimulating both angiogenesis and neurogenesis using hyperbaric oxygen in rats with traumatic brain injury. J. Trauma Acute Care Surg. 72, 650—659.

Lin, A.J., Liu, G., Castello, N.A., Yeh, J.J., Rahimian, R., Lee, G., Tsay, V., Durkin, A.J., Choi, B., LaFerla, F.M., Chen, Z., Green, K.N., Tromberg, B.J., 2014. Optical imaging in an Alzheimer's mouse model reveals amyloid-beta-dependent vascular impairment. Neurophotonics 1, 011005.

Liu, S., Shen, G., Deng, S., Wang, X., Wu, Q., Guo, A., 2013. Hyperbaric oxygen therapy improves cognitive functioning after brain injury. Neural Regen. Res. 8, 3334—3343.

McAlpine, F.E., Lee, J.K., Harms, A.S., Ruhn, K.A., Blurton-Jones, M., Hong, J., Das, P., Golde, T.E., LaFerla, F.M., Oddo, S., Blesch, A., Tansey, M.G., 2009. Inhibition of soluble TNF signaling in a mouse model of Alzheimer's disease prevents preplaque amyloid-associated neuropathology. Neurobiol. Dis. 34, 163—177.

McGeer, P.L., McGeer, E.G., 2015. Targeting microglia for the treatment of Alzheimer's disease. Expert Opin. Ther. Targets 19, 497—506.

Medeiros, R., Kitazawa, M., Passos, G.F., Baglietto-Vargas, D., Cheng, D., Cribbs, D.H., LaFerla, F.M., 2013. Aspirin-triggered lipoxin A4 stimulates alternative activation of microglia and reduces Alzheimer disease-like pathology in mice. Am. J. Pathol. 182, 1780—1789.

Meirovithz, E., Sonn, J., Mayevsky, A., 2007. Effect of hyperbaric oxygenation on brain hemodynamics, hemoglobin oxygenation and mitochondrial NADH. Brain Res. Rev. 54, 294—304.

Mosher, K.I., Wyss-Coray, T., 2014. Microglial dysfunction in brain aging and Alzheimer's disease. Biochem. Pharmacol. 88, 594—604.

Nazem, A., Sankowski, R., Bacher, M., Al-Abed, Y., 2015. Rodent models of neuroinflammation for Alzheimer's disease. J. Neuroinflammation 12, 015—0291.

Oddo, S., Caccamo, A., Shepherd, J.D., Murphy, M.P., Golde, T.E., Kayed, R., Metherate, R., Mattson, M.P., Akbari, Y., LaFerla, F.M., 2003. Triple-transgenic model of Alzheimer's disease with plaques and tangles: intracellular Aβ and synaptic dysfunction. Neuron 39, 409—421.

Oh, K.J., Perez, S.E., Lagalwar, S., Vana, L., Binder, L., Mufson, E.J., 2010. Staging of Alzheimer's pathology in triple transgenic mice: a light and electron microscopic analysis. Int. J. Alzheimer's Dis. 2010, 2010.

Paresce, D.M., Ghosh, R.N., Maxfield, F.R., 1996. Microglial cells internalize aggregates of the Alzheimer's disease amyloid beta-protein via a scavenger receptor. Neuron 17, 553–565.

Pickering, M., O'Connor, J.J., 2007. Pro-inflammatory cytokines and their effects in the dentate gyrus. Prog. Brain Res. 163, 339–354.

Prince, M., Bryce, R., Albanese, E., Wimo, A., Ribeiro, W., Ferri, C.P., 2013. The global prevalence of dementia: a systematic review and metaanalysis. Alzheimers Dement 9, 63–75.

Rama Rao, K.V., Kielian, T., 2015. Neuron-astrocyte interactions in neurodegenerative diseases: role of neuroinflammation. Clin. Exp. Neuroimmunol 6, 245–263.

Rishal, I., Golani, O., Rajman, M., Costa, B., Ben-Yaakov, K., Schoenmann, Z., Yaron, A., Basri, R., Fainzilber, M., Galun, M., 2013. WIS-NeuroMath enables versatile high throughput analyses of neuronal processes. Dev. Neurobiol. 73, 247–256.

Rockswold, S.B., Rockswold, G.L., Zaun, D.A., Liu, J., 2013. A prospective, randomized Phase II clinical trial to evaluate the effect of combined hyperbaric and normobaric hyperoxia on cerebral metabolism, intracranial pressure, oxygen toxicity, and clinical outcome in severe traumatic brain injury. J. Neurosurg. 118, 1317–1328.

Roher, A.E., Debbins, J.P., Malek-Ahmadi, M., Chen, K., Pipe, J.G., Maze, S., Belden, C., Maarouf, C.L., Thiyyagura, P., Mo, H., Hunter, J.M., Kokjohn, T.A., Walker, D.G., Kruchowsky, J.C., Belohlavek, M., Sabbagh, M.N., Beach, T.G., 2012. Cerebral blood flow in Alzheimer's disease. Vasc. Health Risk Manag. 8, 599–611.

Sahni, T., Jain, M., Prasad, R., Sogani, S.K., Singh, V.P., 2012. Use of hyperbaric oxygen in traumatic brain injury: retrospective analysis of data of 20 patients treated at a tertiary care centre. Br. J. Neurosurg. 26, 202–207.

Schneider, J.A., Wilson, R.S., Cochran, E.J., Bienias, J.L., Arnold, S.E., Evans, D.A., Bennett, D.A., 2003. Relation of cerebral infarctions to dementia and cognitive function in older persons. Neurology 60, 1082–1088.

Sheng, J.G., Zhu, S.G., Jones, R.A., Griffin, W.S., Mrak, R.E., 2000. Interleukin-1 promotes expression and phosphorylation of neurofilament and tau proteins in vivo. Exp. Neurol. 163, 388–391.

Shi, J.Q., Shen, W., Chen, J., Wang, B.R., Zhong, L.L., Zhu, Y.W., Zhu, H.Q., Zhang, Q.Q., Zhang, Y.D., Xu, J., 2011. Anti-TNF-alpha reduces amyloid plaques and tau phosphorylation and induces CD11c-positive dendritic-like cell in the APP/PS1 transgenic mouse brains. Brain Res. 12, 239–247.

Simsek, K., Ozler, M., Yildirim, A.O., Sadir, S., Demirbas, S., Oztosun, M., Korkmaz, A., Ay, H., Oter, S., Yildiz, S., 2012. Evaluation of the oxidative effect of long-term repetitive hyperbaric oxygen exposures on different brain regions of rats. ScientificWorldJournal 2012, 849183.

Simsek, K., Sadir, S., Oter, S., 2015. The relation of hyperbaric oxygen with oxidative stress - reactive molecules in action. Oxid Antioxid. Med. Sci. 4, 17–22.

Spangenberg, E.E., Lee, R.J., Najafi, A.R., Rice, R.A., Elmore, M.R., Blurton-Jones, M., West, B.L., Green, K.N., 2016. Eliminating microglia in Alzheimer's mice prevents neuronal loss without modulating amyloid-beta pathology. Brain 139 (Pt 4), 1265–1281.

Sterniczuk, R., Antle, M.C., Laferla, F.M., Dyck, R.H., 2010. Characterization of the 3xTg-AD mouse model of Alzheimer's disease: part 2. Behavioral and cognitive changes. Brain Res. 1348, 149–155.

Tal, S., Hadanny, A., Berkovitz, N., Sasson, E., Ben-Jacob, E., Efrati, S., 2015. Hyperbaric oxygen may induce angiogenesis in patients suffering from prolonged post-concussion syndrome due to traumatic brain injury. Restor Neurol. Neurosci. 4, 43.

Teo, J.D., Morris, M.J., Jones, N.M., 2015. Hypoxic postconditioning reduces microglial activation, astrocyte and caspase activity, and inflammatory markers after hypoxia-ischemia in the neonatal rat brain. Pediatr. Res. 77, 757–764.

Terry, R.D., Gonatas, N.K., Weiss, M., 1964. Ultrastructural studies in Alzheimer's presenile dementia. Am. J. Pathol. 44, 269–297.

Theriault, P., ElAli, A., Rivest, S., 2015. The dynamics of monocytes and microglia in Alzheimer's disease. Alzheimer's Res. Ther. 7, 41.

Thom, S.R., 2009. Oxidative stress is fundamental to hyperbaric oxygen therapy. J. Appl. Physiol. (1985) 106, 988–995.

Thom, S.R., 2011. Hyperbaric oxygen: its mechanisms and efficacy. Plast. Reconstr. Surg. 127.

Thomas, T., Miners, S., Love, S., 2015. Post-mortem assessment of hypoperfusion of cerebral cortex in Alzheimer's disease and vascular dementia. Brain 138 (Pt 4), 1059–1069.

Tian, X., Wang, J., Dai, J., Yang, L., Zhang, L., Shen, S., Huang, P., 2012. Hyperbaric oxygen and Ginkgo Biloba extract inhibit Abeta25-35-induced toxicity and oxidative stress in vivo: a potential role in Alzheimer's disease. Int. J. Neurosci. 122, 563–569.

Tian, X., Zhang, L., Wang, J., Dai, J., Shen, S., Yang, L., Huang, P., 2013. The protective effect of hyperbaric oxygen and Ginkgo biloba extract on Abeta25-35-induced oxidative stress and neuronal apoptosis in rats. Behav. Brain Res. 242, 1–8.

Tibbles, P.M., Edelsberg, J.S., 1996. Hyperbaric-oxygen therapy. N. Engl. J. Med. 334, 1642–1648.

Tikka, T., Fiebich, B.L., Goldsteins, G., Keinanen, R., Koistinaho, J., 2001. Minocycline, a tetracycline derivative, is neuroprotective against excitotoxicity by inhibiting activation and proliferation of microglia. J. Neurosci. 21, 2580–2588.

Tobinick, E., Gross, H., Weinberger, A., Cohen, H., 2006. TNF-alpha modulation for treatment of Alzheimer's disease: a 6-month pilot study. MedGenMed 8, 25.

Tosun, D., Mojabi, P., Weiner, M.W., Schuff, N., 2010. Joint analysis of structural and perfusion MRI for cognitive assessment and classification of Alzheimer's disease and normal aging. Neuroimage 52, 186–197.

Tweedie, D., Ferguson, R.A., Fishman, K., Frankola, K.A., Van Praag, H., Holloway, H.W., Luo, W., Li, Y., Caracciolo, L., Russo, I., Barlati, S., Ray, B., Lahiri, D.K., Bosetti, F., Greig, N.H., Rosi, S., 2012. Tumor necrosis factor-alpha synthesis inhibitor 3,6'-dithiothalidomide attenuates markers of inflammation, Alzheimer pathology and behavioral deficits in animal models of neuroinflammation and Alzheimer's disease. J. Neuroinflammation 9, 106.

van Hulst, R.A., Haitsma, J.J., Klein, J., Lachmann, B., 2003. Oxygen tension under hyperbaric conditions in healthy pig brain. Clin. Physiol. Funct. Imaging 23, 143–148.

Villegas-Llerena, C., Phillips, A., Reitboeck, P.G., Hardy, J., Pocock, J.M., 2015. Microglial genes regulating neuroinflammation in the progression of Alzheimer's disease. Curr. Opin. Neurobiol. 36, 74–81.

Wang, Q., Wu, J., Rowan, M.J., Anwyl, R., 2005. Beta-amyloid inhibition of long-term potentiation is mediated via tumor necrosis. Eur. J. Neurosci. 22, 2827–2832.

Wang, H., Wang, Y., Hong, X., Li, S., 2016. Quantitative proteomics reveals the mechanism of oxygen treatment on lenses of Alzheimer's disease model mice. J. Alzheimer's Dis. 54, 275–286.

Wisniewski, H.M., Wegiel, J., Wang, K.C., Kujawa, M., Lach, B., 1989. Ultrastructural studies of the cells forming amyloid fibers in classical plaques. Can J. Neurol. Sci. 16 (4 Suppl), 535–542.

Yamamoto, M., Kiyota, T., Horiba, M., Buescher, J.L., Walsh, S.M., Gendelman, H.E., Ikezu, T., 2007. Interferon-gamma and tumor necrosis factor-alpha regulate amyloid-beta plaque deposition and beta-secretase expression in Swedish mutant APP transgenic mice. Am. J. Pathol. 170, 680–692.

Yang, L., Tang, J., Chen, Q., Jiang, B., Zhang, B., Tao, Y., Li, L., Chen, Z., Zhu, G., 2015. Hyperbaric oxygen preconditioning attenuates neuroinflammation after intracerebral hemorrhage in rats by regulating microglia characteristics. Brain Res. 19, 21–30.

Yrjanheikki, J., Keinanen, R., Pellikka, M., Hokfelt, T., Koistinaho, J., 1998. Tetracyclines inhibit microglial activation and are neuroprotective in global brain ischemia. Proc. Natl. Acad. Sci. U S A 95, 15769–15774.

Yrjanheikki, J., Tikka, T., Keinanen, R., Goldsteins, G., Chan, P.H., Koistinaho, J., 1999. A tetracycline derivative, minocycline, reduces inflammation and protects against focal cerebral ischemia with a wide therapeutic window. Proc. Natl. Acad. Sci. U S A 96, 13496–13500.

Yu, Y., Matsuyama, Y., Yanase, M., Ito, S., Adachi, K., Satake, K., Ishiguro, N., Kiuchi, K., 2004. Effects of hyperbaric oxygen on GDNF expression and apoptosis in spinal cord injury. Neuroreport 15, 2369–2373.

Zhang, X., Le, W., 2010. Pathological role of hypoxia in Alzheimer's disease. Exp. Neurol. 223, 299–303.